RESPONSIVE POLYMER-GRAFTED CELLULOSE NANOCRYSTALS

RESPONSIVE POLYMER-GRAFTED CELLULOSE NANOCRYSTALS FROM CERIC (IV) ION-INITIATED POLYMERIZATION

By HO MING KEVIN KAN, B.ENG.BIOSCIENCES

A thesis Submitted to the School of Graduate Studies in Partial Fulfillment
of the Requirements for the Degree Master of Applied Science

Master of Applied Science (2013)	McMaster University
(Chemical Engineering)	Hamilton, Ontario

TITLE	Responsive Polymer-Grafted Cellulose Nanocrystals from Ceric (IV) Ion-Initiated Polymerization
AUTHOR	Ho Ming Kevin Kan, B.Eng.Biosciences (McMaster University, Hamilton, Ontario)
SUPERVISOR	Dr. Emily Cranston
NUMBER OF PAGES:	xii, 88

Abstract

In recent years, cellulose nanocrystals (CNCs) isolated from natural cellulosic sources through an acid hydrolysis treatment have garnered significant interest in both academia and industry. CNCs have attracted attention not only because they stem from an abundant, renewable resource and are biodegradable, but also because of their low density, light weight, high aspect ratio, high tensile strength and a specific Young's modulus comparable to steel and Kevlar. These properties make CNCs ideal for use as reinforcing agents in nanocomposites, as well as stabilizing agents in foams and gels. However, due to the high surface area and hydrophilic nature of CNCs, unmodified nanocrystals are difficult to disperse in non-polar materials. The lack of interfacial compatibility between components causes CNCs to agglomerate and thus their incorporation into conventional polymer matrices has been challenging at best, and unsatisfactory in most cases.

In this work, CNCs have been rendered pH and temperature-responsive by surface-initiated graft polymerization of 4-vinylpyridine and *N*-isopropylacrylamide, respectively, using ceric (IV) ammonium nitrate as the initiator. The resultant suspensions of poly(4-vinylpyridine)-grafted cellulose nanocrystals (P4VP-*g*-CNCs) and poly(*N*-isopropylacrylamide)-grafted cellulose nanocrystals (PNIPAM-*g*-CNCs) show reversible hydrophilic to hydrophobic responses with changes in pH and temperature, respectively. The presence of grafted polymer and the tunable hydrophilic/hydrophobic properties were characterized via Fourier transform infrared spectroscopy, elemental analysis, electrophoretic mobility, mass spectrometry, transmittance spectroscopy, contact angle measurements, thermal analysis and various microscopies.

The intention of this work has been to shift towards more industrially viable surface modification routes for CNCs by using a one-pot, water-based synthesis to produce a low cost and functional nanomaterial. Moreover, sonication is used throughout the polymerization reaction to avoid particle aggregation and ensure that individual CNCs are surface-functionalized. As a result, reproducible and uniform material properties have been measured in both suspensions and films of modified CNCs. The responsive nature of P4VP-*g*-CNCs and PNIPAM-*g*-CNCs may offer new applications for cellulose nanocrystals in hydrophobic nanocomposites, biomedical devices, as clarifying agents, and in industrial separation processes.

Acknowledgements

I would like to express my gratitude to my supervisor, Dr. Emily Cranston for her continuous and invaluable assistance, guidance, support and encouragement throughout my graduate studies. Thank you for always being understanding and patient with me. I would also like to acknowledge the Natural Sciences and Engineering Research Council of Canada for financial support of this work.

I would also like to thank the members of the Cranston Research group for all their suggestions and help over these years. This experience would not have been the same without their assistance and the friendships have made this experience memorable. To Dr. Tiffany Abitbol, thank you for all the helpful advice and comments. To Heera Marway, Xuan Yang, Lexa Graham and Jonathan Monster, thank you for all the help and support, especially during the first few months of my studies.

Special thanks to Dr. Robert Pelton, Dr. Carlos Filipe and Dr. Shiping Zhu for access to their instruments and expertise, Mr. Andy Duff, Mr. Frank Gibbs, Ms. Elizabeth Takacs and Dr. Kirk Green for sample analysis training and Dr. Alexander. Wahba for helpful advice in regards to mass spectrometry.

Lastly, I would like to thank my family and friends for their encouragement and support throughout my studies. To my parents, words cannot express my gratitude. To my brother and sister, I’m thankful for your continuous support and advice.

Table of Contents

List of Figures

List of Tables

List of Abbreviations and Symbols

4VP	4-Vinylpyridine
AFM	Atomic Force Microscopy
C	Carbon
CAN	Ceric (IV) Ammonium Nitrate
CAS	Ceric (IV) Ammonium Sulfate
CNCs	Cellulose Nanocrystals
DSA-TOF	Direct Sample Analysis – Time of Flight
DLS	Dynamic Light Scattering
DDLS	Depolarized Dynamic Light Scattering
DMAP	4-Dimethylaminopyridine
DP	Degree of Polymerization
EA	Elemental Analysis
ESEM	Environmental Scanning Electron Microscopy
EO	Ethylene Oxide
FTIR	Fourier Transform Infrared Spectrometry
H	Hydrogen
LCST	Lower Critical Solution Temperature
MCC	Microcrystalline Cellulose
MALDI-TOF	Matrix Assisted Laser Desorption/Ionization – Time of Flight
N	Nitrogen
NIPAM	*N*-isopropylacrylamide
PAA	Poly(acrylic acid)
P4VP	Poly(4-vinyl pyridine)
P4VP-*g*-CNCs	Poly(4-vinyl pyridine)-Grafted Cellulose Nanocrystals
PEG	Poly(ethylene glycol)
PNIPAM	Poly(*N*-isopropylacrylamide)
PNIPAM-*g*-CNCs	Poly(*N*-isopropylacrylamide)-Grafted Cellulose Nanocrystals
PO	Propylene Oxide
POM	Polarized Optical Microscopy
S	Sulfur
SANS	Small Angle Neutron Scattering
SEM	Scanning Electron Microscopy
SI-SET-LRP	Surface Initiated Single Electron Transfer Living Radical Polymerization
TEM	Transmission Electron Microscopy
TEMPO	2,2,6,6-tetramethylpiperidine-1-oxyl
UPy	Ureidopyrimidone
UV	Ultraviolet

1.0 Introduction

1.1 Cellulose

Cellulose, the most abundant biopolymer on Earth, is widely distributed in a variety of living species such as plants, marine animals, fungi and bacteria [1]. Regardless of its source, cellulose is a high molecular weight homopolysaccharide composed of anhydro-D-glucose units where the repeating segment consists of two anhydroglucose units connected by β-1,4 glycosidic linkages. The repeat unit is known as cellobiose and is shown in Figure 1. Each cellulose chain consists of a chemically reducing functionality at one end (a hemiacetal unit), and a nonreducing end, with pendant hydroxyl groups [2]. In addition, each anhydroglucose unit has three hydroxyl groups, including a primary alcohol group at the C_6 position and two secondary alcohol groups at the C_2 and C_3 positions.

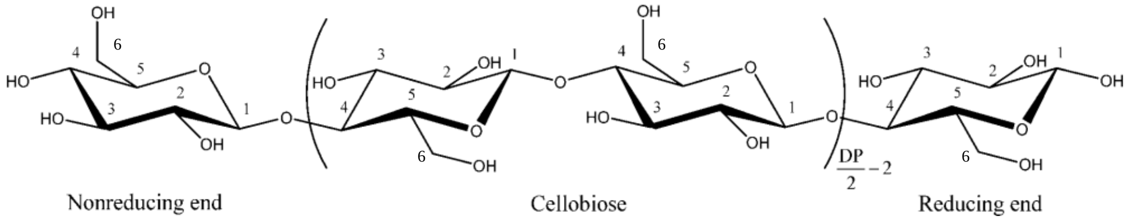

Figure 1. The chemical structure of cellulose. Figure adapted from reference [2].

In nature, cellulose chains associate through van der Waals forces and both inter- and intra-molecular hydrogen bonds to form hierarchical assemblies [2]. At the site of biosynthesis, individual cellulose chains are brought together to form larger units known as elementary fibrils (protofibrils) which further aggregate into larger units called microfibrils and then assemble into cellulose fibers [3]. These cellulose fibers are the main reinforcement phase for many living species such as trees and plants, as well as some bacteria that secrete cellulose fibers to create external network structures. Cellulose fibres consist of alternating highly ordered crystalline regions, where cellulose chains are tightly packed and stabilized by hydrogen bonds, and less ordered amorphous-like regions [4]. Different sources of cellulose exhibit different packing which is dictated by the biosynthetic process and as such, the crystal structure and distribution of ordered and disordered domains varies [5].

1.2 Cellulose Nanocrystals

Cellulose nanocrystals (CNCs) are rigid, rod-like particles produced from natural cellulose sources with widths of a few nanometers and lengths ranging from hundreds of nanometers to microns [2]. In recent years, CNCs have attracted significant attention not only because of their renewability and biodegradability but also because of other attractive properties such as low density, light weight, high aspect ratio, mechanical strength and unique optical properties [2–4,6,7].

1.2.1 Preparation of Cellulose Nanocrystals

Cellulose nanocrystals are generally isolated from cellulose through an acid hydrolysis process which removes the more accessible amorphous regions and leaves intact the highly crystalline regions that are more resistant to acid degradation (Figure 2) [8–10]. The dimensions, crystallinity and colloidal stability of CNCs depend primarily on the cellulose source and the acid hydrolysis conditions [2]. Rånby [8] and Battista [11] were the first to produce stable CNC suspensions from the sulfuric acid hydrolysis of cellulose. Some decades later, Dong *et al*. [10] studied the hydrolysis conditions in detail and observed that longer reaction times led to shorter nanocrystals with greater surface charge [10]. Later, research conducted by Azizi Samir *et al*. [12] reported that the acid concentration affected the morphology of the nanocrystals extracted from sugar beet, specifically. Beck-Candanedo *et al*. [9] investigated the reaction time and acid-to-pulp ratio of softwood and hardwood cellulose sources, and confirmed that the reaction time was the most influential parameter during acid hydrolysis. Similar to the previous findings, longer hydrolysis times produced shorter nanocrystals with narrower polydispersity, however, an excessively long reaction time eventually digested the cellulose into its component glucose units [9,10]. Elazzouzi-Hafraoui *et al*. [13] studied the effect of sulfuric acid temperature on the hydrolysis of cotton and demonstrated that a higher temperature produced shorter nanocrystals. Overall, the dimensions of CNCs were found to be smaller when harsher hydrolysis conditions were employed (e.g., high acid-to-cellulose ratio, high temperature and long reaction times) [6,14,15].

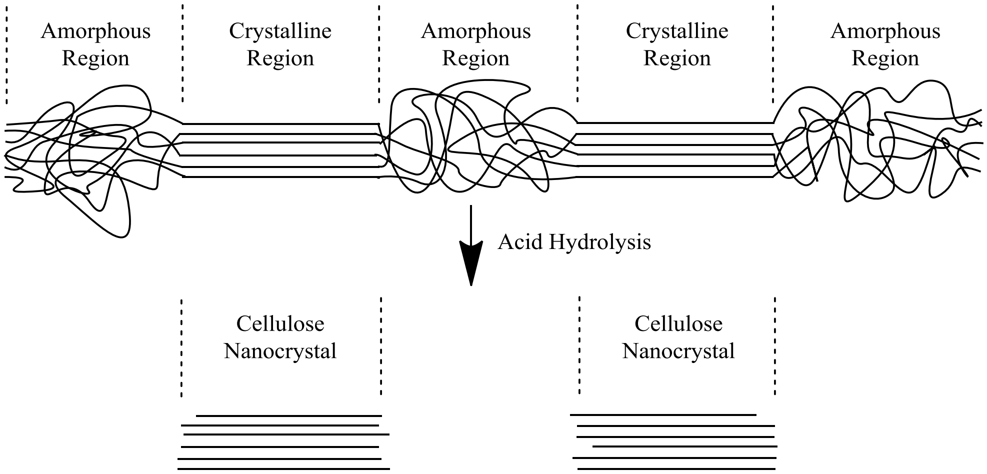

Figure 2. Schematic of a cellulose microfibril with crystalline and amorphous regions and the resulting cellulose nanocrystals after acid hydrolysis.

Sulfuric acid is by far the most common acid used to produce CNCs although other concentrated mineral acids such as hydrochloric, phosphoric and hydrobromic acid have also been reported [2]. Figure 3a shows the acid hydrolysis mechanism of cellulose in sulfuric acid which involves the protonation of the glycosidic oxygen (path 1) or the cyclic oxygen (path 2) from the hydronium ion. This leads to the hydrolytic cleavage of the glycosidic bonds by the addition of water [16]. Overall, the acid hydrolysis leads to smaller fragments of cellulose chains where the cellulose backbone is preserved. The use of sulfuric acid as a hydrolyzing agent has also been shown to react with the surface hydroxyl groups to form negative sulfate ester groups as shown in Figure 3b [6,14,16]. These anionic groups electrostatically stabilize CNCs in aqueous suspension and prevent agglomeration through electrostatic double layer repulsion [10,17]. Acid hydrolysis with hydrochloric acid, on the other hand, yields uncharged CNCs which tend to flocculate in aqueous suspension [18].

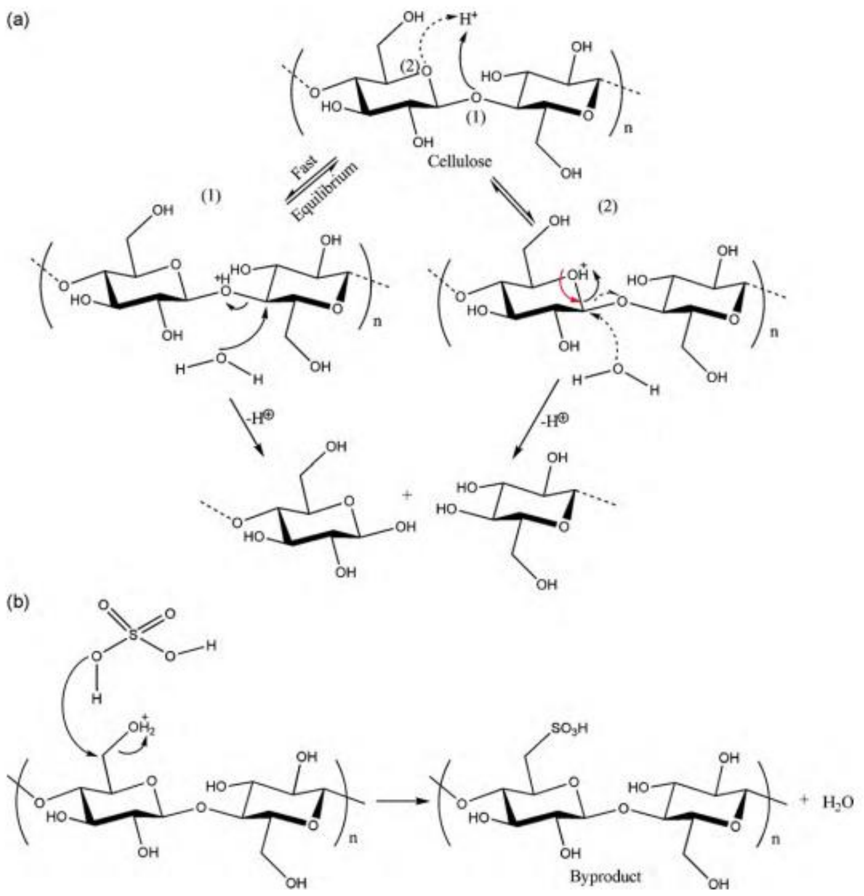

Figure 3. Schematic diagram illustrating (a) the mechanism of acid hydrolysis and (b) esterification of CNCs. Figure reproduced from reference [16].

1.2.2 Morphological Properties of Cellulose Nanocrystals

The morphology of CNCs is typically studied by microscopy, including transmission electron microscopy (TEM), scanning electron microscopy (SEM), and atomic force microscopy (AFM). Light scattering techniques, such as small angle neutron scattering (SANS) and polarized and depolarized dynamic light scattering (DLS/DDLS) have also been used. TEM micrographs of CNCs produced from different cellulose sources are shown in Figure 4, and the dimensions of CNCs from different sources determined using various techniques is presented in Table 1. Generally, CNCs isolated from bacteria and tunicate (a marine invertebrate) are longer than those produced from plant-based cellulose such as cotton and wood. This is because of the very high purity and crystallinity of cellulose from bacteria and tunicate, which is therefore broken down to a lesser extent by acid hydrolysis. Furthermore, the aspect ratio (defined as the length-to-width ratio) ranges from 10–30 for cotton and up to approximately 70 for CNCs from tunicate [19,20].

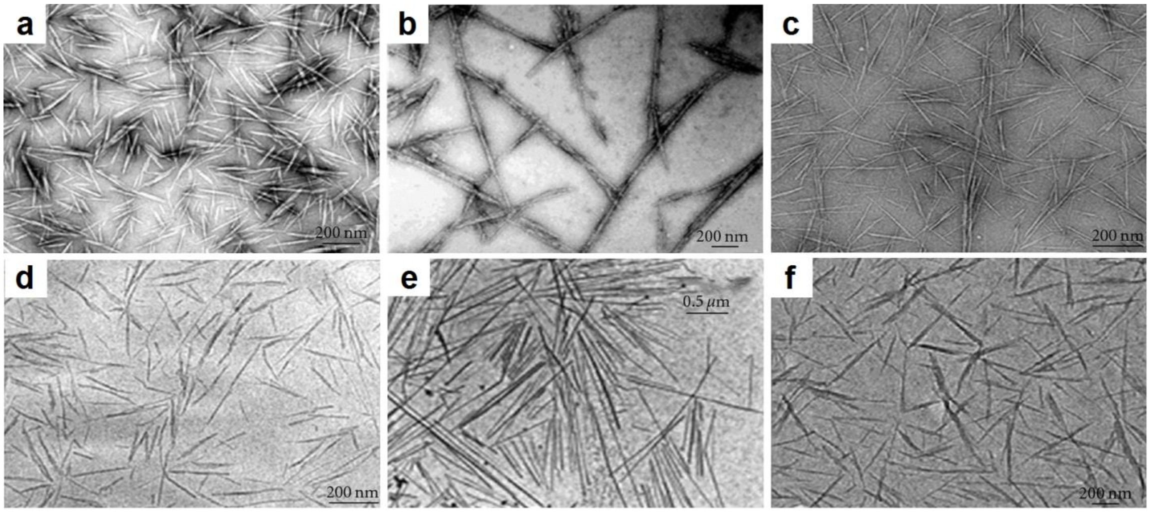

Figure 4. Transmission electron micrographs of cellulose nanocrystals from (a) ramie [14], (b) bacteria [21], (c) sisal [22], (d) sugar beet pulp [12], (e) tunicate [19] and (f) cotton [23]. Figure adapted from reference [24].

Table 1. Dimensions of cellulose nanocrystals from various sources measured using different techniques.

Source	Length (nm)	Cross-section (nm)	Technique	Reference
Bacterial	100–1000	10–50	TEM	[25]
	100–several μm	10–50 × 30–50	TEM	[21]
Cotton	100–150	5–10	TEM	[18]
	255	15	DDLS	[20]
Luffa Cylindrical	242	5	TEM	[26]
Microcrystalline Cellulose (MCC)	~ 500	10	AFM	[27]
	150–300	3–7	TEM	[28]
Ramie	150–250	6–8	TEM	[14]
Sisal	100–500	3–5	TEM	[22]
Sugar Beet Pulp	210	5	TEM	[12]
Tunicate	1160	16	DDLS	[20]
	500–2000	10	TEM	[19]
Wheat Straw	150–300	5	TEM	[29]
Soft Wood	100–150	4–5	AFM	[9]
Hard Wood	140–150	4–5	AFM	[9]

1.3 Chemical Modifications of Cellulose Nanocrystals

CNCs from sulfuric acid are often referred to as either “acid-form” or “sodium-form”, depending on the nature of the counterion associated with the surface sulfate ester group. Unmodified, acid-form CNCs that have been freeze or spray dried cannot be re-dispersed due to strong cellulose-cellulose interactions and interparticle hydrogen bonding [30–32]. While it is possible to redisperse the dried sodium-form of CNCs into polar solvents, the hydrophilicty of CNCs makes it extremely challenging to uniformly disperse unmodified CNCs in hydrophobic solvents and polymers [7]. Chemical modification of the abundant and accessible surface hydroxyl groups on CNCs is a good way to overcome the dispersion challenge. Both noncovalent and covalent surface modifications have been reported in the literature with the focus on improving the dispersibility and compatibility of CNCs in different matrices primarily for use in nanocomposites. Noncovalent surface modification are generally carried out by the adsorption of polyelectrolytes or surfactants, whereas a seemingly limitless range of covalent chemical modifications of CNCs is possible, including sulfonation, oxidation [33], cationization [34], silylation [35], and grafting via acid chlorides [36], acid anhydrides [37] or isocyanates [38], as depicted in Figure 5.

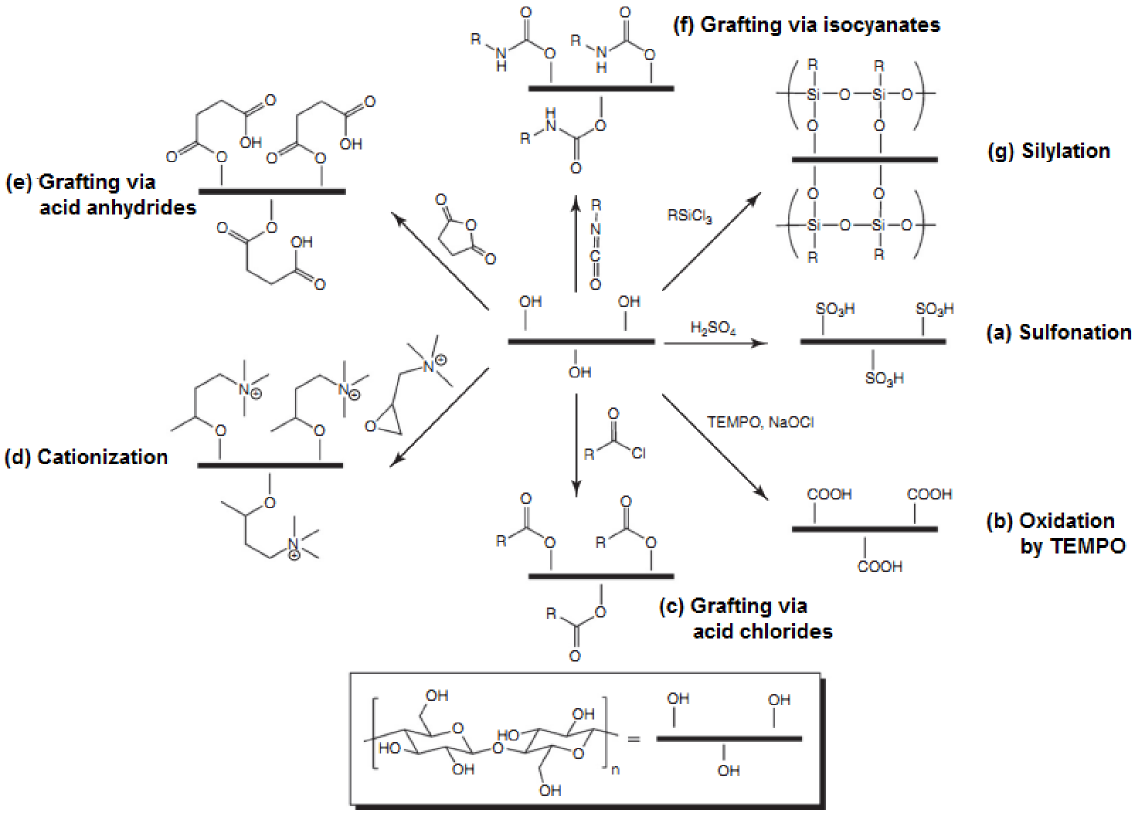

Figure 5. Schematic diagram illustrating various CNC surface modifications [33–38]. Figure adapted from reference [39].

1.3.1 Polymer Grafting

The agglomeration of CNCs in aqueous and organic suspensions can be prevented by surface modifications that lead to steric stabilization, such as grafting polymer brushes onto CNC surfaces [18,40]. However, the drawback of most chemical modifications presented in the literature is that they are performed in organic media and require a tedious and lengthy solvent exchange process to temporarily suspend the CNCs in solution. The grafting of polymers on the surface of CNCs can be performed by two techniques, namely, "grafting-to" and "grafting-from" as shown in Figure 6 [41]. "Grafting-to" involves the attachment of pre-synthesized and characterized polymer chains to the hydroxyl groups of the CNC surface. Conversely, "grafting-from" involves the surface initiated, *in-situ* polymerization from initiators immobilized on the surface, to generate tethered polymers by conventional free radical [42] ionic [27] or ring-opening polymerizations [14,43].

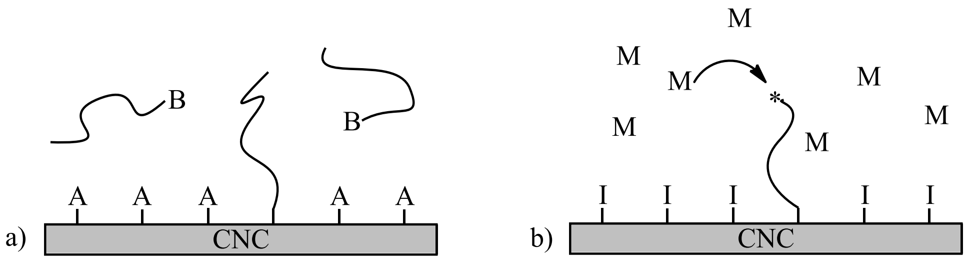

Figure 6. Grafting of polymer brushes on CNCs by (a) the "grafting-to" approach whereby pre-synthesized polymer with end-functionality "B" react with CNC surface "A" groups and (b) the "grafting-from" approach whereby polymers are grown from surface-immobilized initiators (I) by adding monomers (M) to the growing polymer chain active site (*).

1.4 Stimuli-Responsive Polymers

In recent years, tailored molecular assemblies and interfaces with specific chemical functionality and structure have been constructed for a variety of applications, including “smart” materials, controlled drug delivery, and environmentally-responsive coatings [44,45]. External environmental cues include temperature [40,46–48], pH [49,50], chemical composition, humidity, applied mechanical forces, exposure to irradiation [51], exposure to an electric or magnetic field, etc. These cues can trigger conformational and chemical changes which lead to modified chemical, mechanical and optical properties for different stimuli-responsive macromolecular nanostructures.

An overview of stimuli-responsive nanostructured polymer materials and systems in thin films and nanoparticles is shown in Figure 7. Generally, stimuli-responsive polymer materials are classified into the categories of [44]:

1. Polymer surfaces formed in bulk polymer materials
2. Grafted polymer thin films (may also be referred to as polymer brushes)
3. Thin films and membranes of polymer networks
4. Self-assembled multilayer thin films

Factors that must be considered when comparing different stimuli-responsive polymers include the rate of response, the amplitude of change of material properties, reversibility, and the intensity of external signal needed to trigger a response [44]. Normally, bulk polymers have long response times, ranging from minutes to hours, while thin polymer coatings have rapid response rates with the mechanical properties of the bulk polymer retained [52]. In some cases, the response times of thin polymer films can also be finely tuned to range from seconds to hours [44].

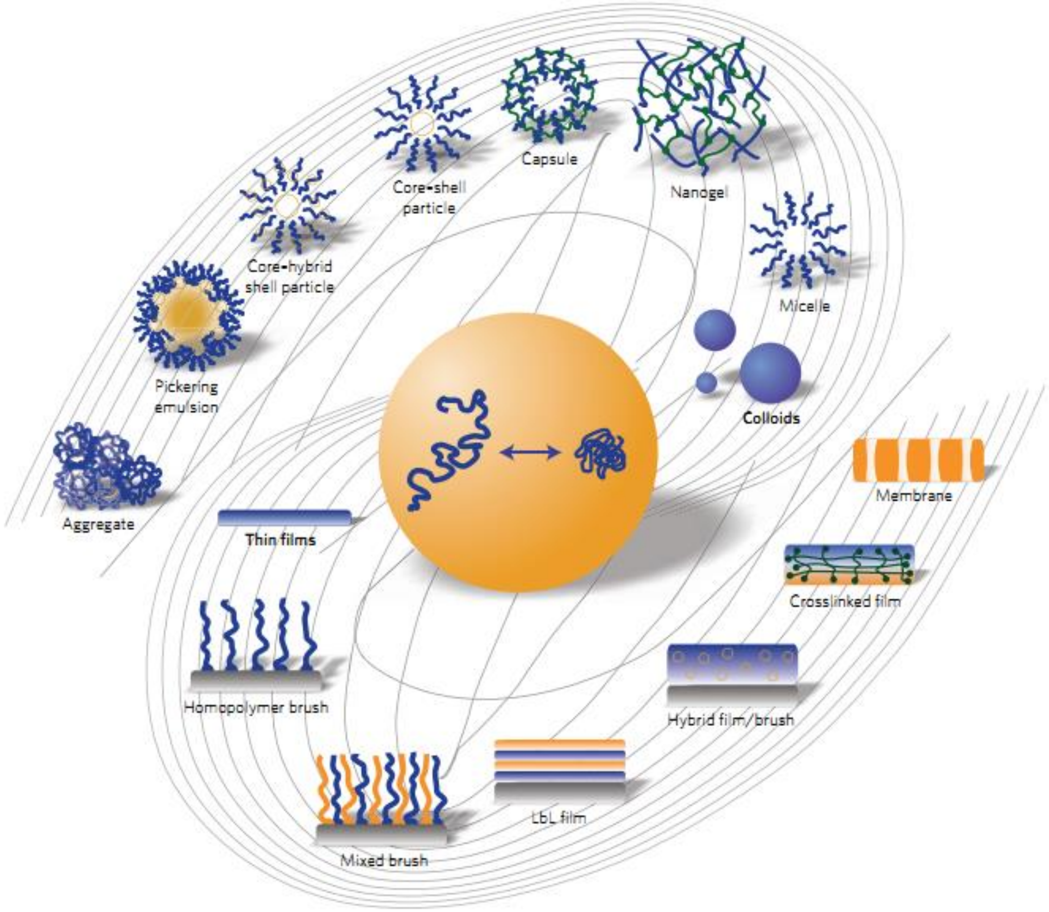

Figure 7. Nanostructured stimuli-responsive polymer materials that rely on the phase behavior of macromolecular assemblies in thin films (polymer brushes, multilayer films, hybrid systems and thin crosslinked and membrane films) and nanoparticles (micelles, nanogels, capsules, core-shell particles, core-hybrid shell particles and their assemblies in solutions and at interfaces in emulsions and foams). Figure reproduced from reference [44].

Both the “grafting-from” and “grafting-to” approaches have been used to prepare adaptive and responsive interfaces that reversibly switch due to external stimuli. Uniform [53,54], patterned [55], and gradient brushes where the grafting density and/or chemical composition gradually changes [56,57] have been reported in literature on both planar and curved surfaces. Furthermore, homopolymer brushes, block copolymer brushes and mixed polymer brushes, as shown in Figure 8, are the possible architectures available to grafted polymers which exhibit responsive behaviours.

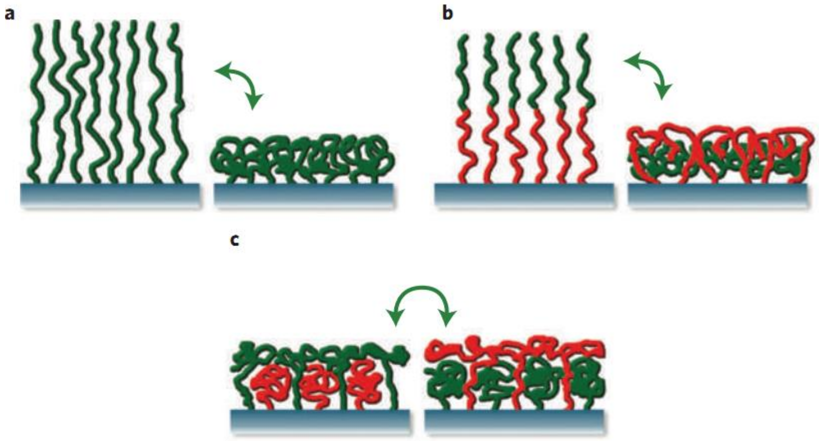

Figure 8. Illustrations of various architectures and responsive behaviour of grafted polymers including (a) homopolymer brushes (b) block copolymer brushes and (c) mixed brushes. Figure reproduced from reference [44].

Figure 8a illustrates single component homopolymer brushes grafted on a planar surface in which the responsiveness of the film originates from the properties of the grafted polymer and its grafting density. For example, the thermoresponsive polymer poly(*N*-isopropylacrylamide) (PNIPAM) possesses a lower critical solution temperature (LCST) around 32°C in aqueous solution [58]. PNIPAM contains hydrophobic and hydrophilic domains which rearrange depending on the water content of the material, the surrounding media (air or liquid) and the ambient temperature. Generally, PNIPAM surfaces appear hydrophilic below the LCST as there is efficient hydrogen bonding with the solvent while above the LCST, dried PNIPAM surfaces are more hydrophobic as intramolecular hydrogen bonds are formed and a phase transition occurs from the increased hydrophobicity [59–61]. The grafting of PNIPAM to different substrates has been used to fabricate functional surfaces with reversible hydrophilic to hydrophobic transitions with changes in temperature [62,63].

Aside from thermosensitive polymers, other responsive polymers include poly(acrylic acid) (PAA) and poly(4-vinylpyridine) (P4VP), which respond to changes in pH. PAA is hydrophobic at $pH < 4$ and becomes hydrophilic after deprotonation ($pH > 4$) [64], whereas P4VP is hydrophilic at $pH < 5$ and becomes hydrophobic after deprotonation ($pH > 5$) [65,66]. While a surface is normally considered hydrophobic if it has a water contact angle greater than 90°, in the work, the precipitation is considered hydrophobic.

Block copolymer brushes grafted to various substrates are another possible architecture for polymer thin films (Figure 8b). The responsiveness of these films are based on the phase segregation of each of the polymer blocks and the combination of these polymeric blocks often results in the surface properties switching from a property of one polymer to another property of the second polymer, or an intermediate state exhibiting properties of both polymers [44]. An example is the grafting of P4VP and PNIPAM block copolymers from cellulose filter paper surfaces using surface initiated atom transfer radical polymerization to produce dual-responsive (both pH and temperature sensitive) cellulose surfaces [65]. These surfaces respond to changes in pH and temperature, which cause the wettability of the surfaces to alternate between the extremes of highly hydrophilic to highly hydrophobic. The different conformations of the dual-responsive block copolymer brushes grafted on macroscopic cellulose surfaces are shown in Figure 9.

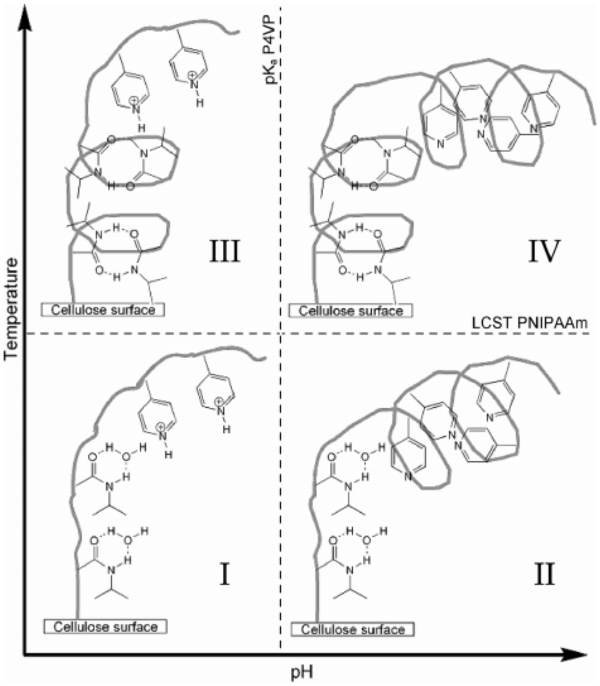

Figure 9. Different conformations of the dual-responsive block copolymer brushes of poly(4-vinylpyridine) and poly(*N*-isopropylacrylamide) at different pH and temperature. The conformation depicted in I is the most hydrophilic and the conformation in IV is the most hydrophobic, with III and IV possessing intermediate wettability. Figure reproduced from reference [65].

Another type of grafting architecture is mixed polymer brushes (Figure 8c), where at least two chemically different polymers are grafted to the same substrate. Similar to block copolymers, phase segregation causes the spatial distribution of the polymer brushes to change at the brush surface resulting in switchable properties. The surface composition and related physical changes of the mixed brushes is the basic mechanism responsible for the modified interactions between the mixed polymer-grafted surface and the environment [44]. One example is the grafting of polystyrene and poly(2-vinyl pyridine) brushes on silicon wafers to prepare mixed polymer brushes. Changes in surface composition and wetting behaviour were observed after rinsing the grafted surfaces in different solvents [53].

1.5 Stimuli-Responsive CNC Suspensions, Gels and Nanocomposites

1.5.1 Grafting of Stimuli-Responsive Polymers to CNCs

Stimuli-responsive polymers have been grafted onto CNCs using both the “grafting-to” and “grafting-from” techniques. Thermo-sensitive amine-terminated statistical copolymers of ethylene oxide (EO) and propylene oxide (PO) (Jeffamines) have been grafted to CNC by a peptide coupling reaction which led to unusual CNC suspension properties such as high ionic strength, surface activity and thermoreversible aggregation [67]. As Jeffamine copolymers generally exhibit thermosensitive behavior, with an LCST that depends on the EP/PO ratio; above this LCST, Jeffamine copolymers reversibly change from a swollen coil to a collapsed globule [68], and this thermosensitive behavior was also observed on the grafted CNCs.

In another example, PNIPAM has been grafted from the surface of CNCs via surface-initiated single-electron transfer living radical polymerization with the use of ethyl 2-bromoisobutyrate as an initiator to produce thermoresponsive polymer brushes on the CNCs [40,69,70]. The thermoresponsive behavior and aggregation of the PNIPAM grafted CNCs were observable by light scattering, rheology and colloidal probe atomic force microscopy. Light transmittance also showed a temperature dependent aggregation above the LCST of the PNIPAM brushes [69].

The grafting of polyethylene glycol (PEG) onto the surface of carboxylated CNCs by the direct condensation of PEG onto the CNC backbone has also been shown to produce solid-solid phase changing materials [48]. Although PEG has been grafted to CNCs by a number of researchers [18,71], the increased thermal conductivity and thermal energy storage of PEG grafted cellulose nanocrystals was only recently studied for applications in phase changing responsive materials. Another more recent study grafted populations of complementary single stranded oligonucleotides (DNA) to CNCs [72]. Combining the populations led to hybridized and self-assembled nanostructures that were reversible by increasing the temperature above the melting temperature of the duplexed DNA.

1.5.2 Stimuli-Responsive CNC Gels

As mentioned, CNC suspensions prepared by sulfuric acid hydrolysis are stable due to the electrostatic repulsion of the negatively charged sulfate ester groups. However, if the stability of the CNC suspensions decreases, for example through a loss or screening of surface charge, CNC suspensions may gel. A number of physical and chemical processes can lead to the gelation of CNCs, including exchanging the counterions associated with the charged ester groups from monovalent to divalent ions [31], increasing the ionic strength of the CNC suspension [73], functionalizing the surface of the CNCs with cationic hydroxypropyltrimethylammonium chloride [34] and evaporating water from aqueous glycerol suspensions of CNCs [74].

CNC gels that are sensitive to pH can be prepared by functionalizing the surface of the CNCs with either carboxylic acid or amine moieties [49]. Above pH ~3, carboxylated CNCs are deprotonated and form aqueous suspensions in water due to the electrostatic double layer repulsion between the negatively charged carboxylic moieties. Conversely, at a low pH, carboxylated CNCs are protonated and an attractive interaction occurs through hydrogen bonding between the surface hydroxyl and carboxylic acid groups leading to hydrogel formation. The opposite pH sensitivity is apparent for amine functionalized CNCs where higher pH results in hydrogel formation and an aqueous suspension is formed at low pH. Following this, pH-responsive carboxylated CNCs have been used as reinforcing agents in PNIPAM-based thermal/pH sensitive hydrogels [75].

1.5.3 Stimuli-Responsive Nanocomposites with CNCs

One promising potential application of CNCs is as a reinforcing agent in nanocomposite materials, as CNCs exhibit high stiffness (an axial Young's modulus ~ 143 GPa [76]) and nanometer scale dimensions. The first example was introduced by Favier *et al*. [77], who used CNCs as a reinforcing agent for poly(styrene-*co*-butyl acrylate) and since then, CNCs have been incorporated as the load-bearing component into a wide range of polymer matrices [2,78].

1.5.3.1 Stimuli-Responsive CNC Fillers

Specifically, CNCs with surface sulfate ester groups have been used as stimuli-responsive fillers to create mechanically adaptive polymer nanocomposites which exhibit changes in stiffness when exposed to aqueous environments [79–81]. A schematic representation of this reversible stiffness mechanism for ethylene oxide-epichlorohydrin copolymer and polyvinyl acetate reinforced with CNCs is shown in Figure 10.

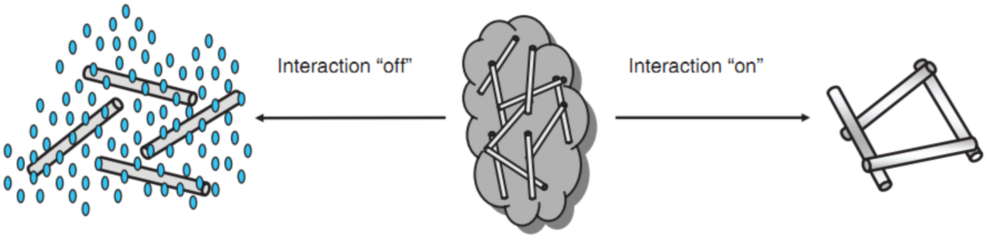

Figure 10. Schematic of the switching mechanism of nanocomposites reinforced with cellulose nanocrystals. Figure reproduced from reference [79].

The switching mechanism of the nanocomposites presented in Figure 10 entails an “on” state and an “off” state. In the “off” state, the nanocomposite is exposed to an aqueous environment and the CNC self-interactions are “switched off”, as there are competitive bonds formed with the solvent. With the evaporation of the solvent, the self-interactions of the CNCs are “switched on” and the CNCs form a rigid, percolating network. This maximizes the stress transfer within the nanocomposite and increases the overall modulus of the nanocomposite [79]. This switching mechanism behavior was apparent for a range of different polymer matrices with sulfated CNCs as a filler [80,81]. Furthermore, other than sulfated CNCs, pH responsive CNCs functionalized by Way *et al*. [49] can be incorporated into poly(vinyl acetate) matrices to yield pH-responsive nanocomposite films. The mechanical properties of these nanocomposites are also influenced in both dry and water swollen states via the pH.

1.5.3.2 Stimuli-Responsive Nanocomposites Reinforced with CNCs

Stimuli-responsive nanocomposites with CNCs as reinforcing fillers have also been reported. Unmodified CNCs were used to reinforce a thermally healable supramolecular polymer formed via π-π interactions between an oligomer terminated at both ends with π-electron rich pyrenyl moieties and a chain-folding oligomer containing pairs of π-electron poor naphthalene-diimide units [82]. It was found that all cellulose reinforced nanocomposites could be repaired after damage when exposed to elevated temperatures, and that reinforcement with CNCs greatly enhanced the mechanical properties. Light-healable, supramolecular nanocomposites reinforced with CNCs have also been reported based on a telechelic poly(ethylene-co-butylene) functionalized with hydrogen-bonding ureidopyrimidone (UPy) and CNCs functionalized with the same binding motif [83]. The reinforced nanocomposites displayed improved mechanical properties and when exposed to ultraviolent radiation, the UPy motifs cause a temporary disengagement of the hydrogen-bonding motifs resulting in a reversible decrease of the supramolecular polymers' molecular weight and viscosity.

1.6 Ceric (IV) Ion-Initiated Polymerization

Of all the polymer "grafting-from" methods, one of the most interesting uses the ceric-cerous redox system to initiate polymerization from pre-existing polymers such as cellulose. Free radicals are formed at the cellulose backbone through the direct oxidation of cellulose, a single electron transfer process whereby electrons are transferred from the hydroxyl group of cellulose to the ceric ion [84,85]. Graft polymerization is then initiated at these radical sites. Mino and Kaizerman [86] were the first to discuss graft polymerization with the use of ceric ions, while Schwab *et al*. [87] were the first to extend this grafting knowledge to cellulose. From then, the grafting of vinyl monomers with the use of this technique has been extended to not only other cellulosic materials such as cotton, wood pulp, paper, rayon, jute, ramie and cellophane, but also other natural and modified polysaccharides [84,88].

1.6.1 Reaction Mechanism

The mechanism proposed by Ogiwara *et al*. [89], for the grafting of vinyl monomers from cellulose with ceric ion-initiation, is presented in the reaction scheme below:

Initiation:

$$\text{Ce(IV)} + \text{Cellulose–H} \overset{K}{\leftrightarrow} \text{Complex} \overset{k_d}{\rightarrow} \text{Cellulose}^{*} + \text{Ce(III)} + \text{H}^{+} \tag{1}$$

$$\text{Cellulose}^{*} + \text{M} \overset{k_i}{\rightarrow} \text{Cellulose–M} \tag{2}$$

$$\text{Ce(IV)} + \text{M} \overset{k_i{}'}{\rightarrow} \text{M}^{*} + \text{Ce(III)} + \text{H}^{+} \tag{3}$$

Propagation:

$$\text{Cellulose–M}^{*}{}_{n} + \text{M} \overset{k_p}{\rightarrow} \text{Cellulose–M}^{*}{}_{n+1} \tag{4}$$

$$\text{M}^{*}{}_{m} + \text{M} \overset{k_p{}'}{\rightarrow} \text{M}^{*}{}_{m+1} \tag{5}$$

Termination:

$$\text{Cellulose–M}^{*}{}_{n} + \text{Ce(IV)} \overset{k_t}{\rightarrow} \text{Cellulose–M}_{n} + \text{Ce(III)} + \text{H}^{+} \tag{6}$$

$$\text{M}^{*}{}_{m} + \text{Ce(IV)} \overset{k_t{}'}{\rightarrow} \text{M}_{m+1} + \text{Ce(III)} + \text{H}^{+} \tag{7}$$

$$\text{Cellulose–M}^{*}{}_{n} + \text{Cellulose}^{*} \overset{k_t{}''}{\rightarrow} \text{Stabilization} \tag{8}$$

$$\text{Cellulose}^{*} + \text{Ce(IV)} \overset{k_0}{\rightarrow} \text{Oxidation Products} + \text{Ce(III)} + \text{H}^{+} \tag{9}$$

Overall, this reaction mechanism is similar to that proposed by Katai *et al*. [90] for the ceric oxidation of alcohols. Other researchers in the field of grafting polymers onto cellulosics have also proposed similar mechanisms [91,92].

Cellulose contains several possible sites for the oxidation by ceric ions. This includes the hydroxyl at C_6, the glycol group at the C_2-C_3 position, the hydroxyl group at the end of the cellulose chain, along with the hemiacetal unit. Many researchers have examined the relative rates of oxidation of these sites using model compounds and Iwakura *et al*. [93] reported that primary alcohols and 1,2 glycols were the most effective oxidation sites while examining the polymerization of polystyrene from various alcohols initiated by ceric ions. Hintz *et al*. [94] also reported that the oxidation of cellulose with ceric ions is more likely to occur at the C_2-C_3 positions and not at the C_6 position. Their work examined the relative rates of oxidation of the C_6 hydroxyl and the C_2-C_3 glycol using model compounds; cyclohexanemethyl alcohol and tetrahydropyran-2-methyl alcohol tested the C_6 hydroxyl and trans-1,2-cyclohexanediol tested the C_2-C_3 glycol. This greater reactivity of the C_2-C_3 glycol has also been reported by other researchers [95].

Furthermore, the oxidation at the hemiacetal unit has also been investigated. Model compounds containing a hemiacetal group similar to cellulose were found to be more readily oxidized than compounds with the hemiacetal group blocked, such as grafting methyl methacrylate to the C_1 position of glucose [96,97]. Pottenger *et al*. [98] studied model compounds for cellulose and reported that the rate of oxidation of the hemiacetal unit was 360 times greater than that of the C_2-C_3 hydroxyl group. However, due to the large number of C_2-C_3 hydroxyl groups on the model compounds, these hydroxyl groups remain highly probable reaction sites.

To understand the mechanism of ceric ion initiation, many quantitative studies have been undertaken with organic compounds that are susceptible to this oxidation reaction. Mino and Kaizerman [95] studied the oxidization of pinacol by ceric sulfate as shown in the reaction below. It was found that the oxidation of one mole of pinacol led to two moles of acetone, and when acrylamide was present only one mole of acetone was produced, as all the free radicals generated led to the initiation of acrylamide polymerization [95]. Overall, these results are expected to translate to cellulose, as the free radicals formed will lead to the grafting of polymer chains when polymerizable monomers are present.

$$Ce^{4+} + C_6H_{14}O_2 \rightarrow (CH_3)_2CO + (CH_3)_2C^{*}OH + H^{+} + Ce^{3+} \qquad (10)$$

$$Ce^{4+} + (CH_3)_2C^{*}OH \rightarrow (CH_3)_2CO + H^{+} + Ce^{3+} \qquad (11)$$

Depending on the site of oxidation, two similar mechanisms for the oxidation by ceric ions at the hemiacetal unit and the C_2-C_3 position have been proposed and supported by others working with cellulosic materials [98–100]. Figure 11 illustrates the oxidation of the hemiacetal unit as proposed by Pottenger *et al*. [98] based on examining the products of the oxidation of glucose by ceric ions in perchloric acid. It was proposed that the C_1-C_2 bond was broken and that the free radical would be formed at the C_1 position due to the greater possibility of resonance stabilization. Analysis of the grafted polymer also showed the presence of an aldehyde group which further confirmed that the C_1-C_2

bond was broken [100]. Furthermore, Pottenger *et al*. [98] also proposed a mechanism for the C_2-C_3 position from examining the products of oxidation for Schardinger β-dextrin and cellulose as shown in Figure 12. This mechanism corresponds to a similar mechanism proposed by Arthur *et al*. [99] which came from examining the oxidation of cotton and microcrystalline cellulose by electron spin resonance (ESR). Overall, both mechanisms suggest that the ceric ion forms a chelated complex with the cellulose molecule in which a transfer of electrons from cellulose to Ce(IV) occurs. This leads to the reduction of Ce(IV) to Ce(III), a breakage of a bond on the cellulose and the formation of a radical. Additionally, it has also been proposed by Kulkarni *et al*. [96,101] from the investigation of the products of cellulose from ceric oxidation that the reaction occurs rapidly due to the formation of the ceric-cellulose complex and oxidation of the hemiacetal units. Thereafter, depending on the oxidation conditions, the oxidation may occur at the C_2 position without the cleavage of the C_2-C_3 bond or proceed through the cleavage of the C_2-C_3 bond.

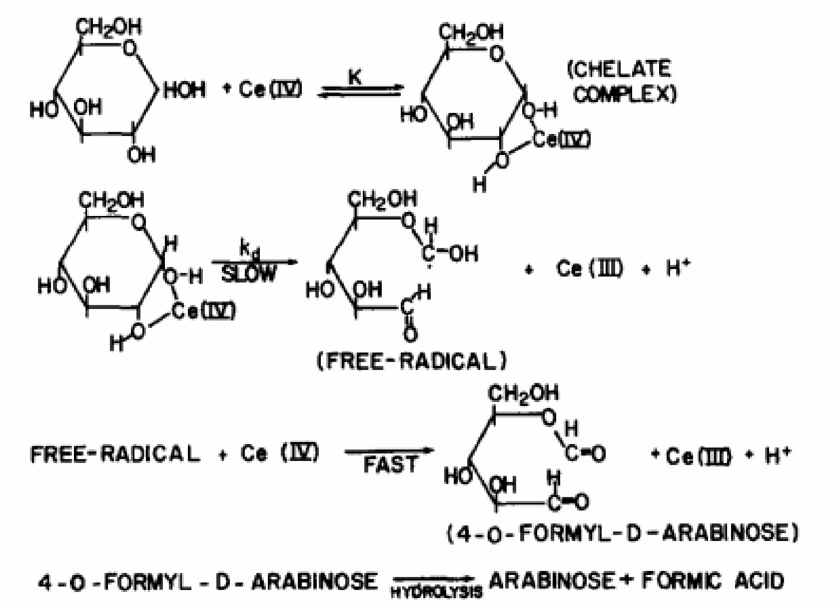

Figure 11. Schematic of the oxidation of the hemiacetal unit for cellulose. Figure reproduced from reference [98].

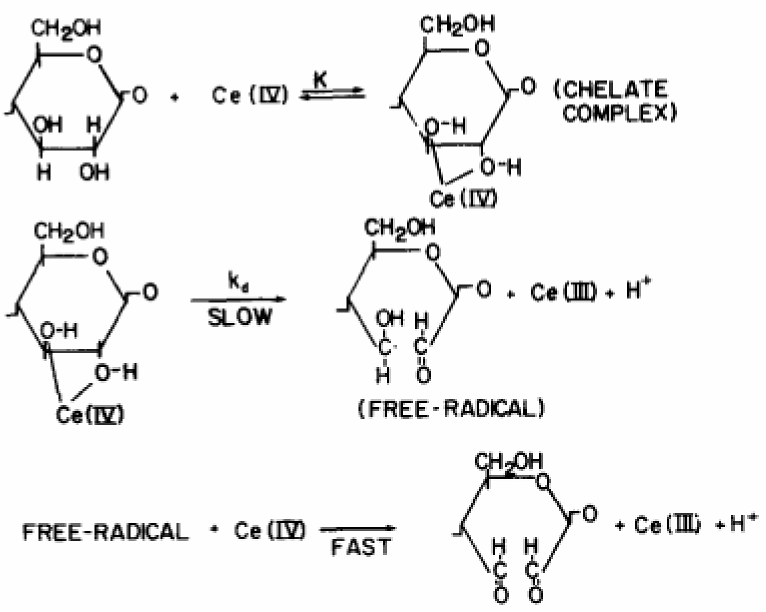

Figure 12. Schematic of the oxidation of the C_2-C_3 position for cellulose. Figure reproduced from reference [98].

Aside from the free-radical mechanism shown previously, an alternative mechanism for the grafting of polar vinyl monomers to cellulosics has been proposed by Gaylord *et al*. [102,103] This mechanism focuses on cellulose-monomer interactions or complexations, where cellulose acts as a complexing agent for the activation of acceptor monomers and the alignment of monomer-cellulose-water donor-acceptor complexes. The grafting of polymer chains and homopolymerization are products of the addition of monomer-cellulose-water complexes by a non-radical mechanism. All in all, although this mechanism is of considerable interest, more experimental justification is needed and currently no single mechanism has been generally accepted [84].

1.6.2 Grafting Parameters

Due to the heterogeneity of the reaction, the number of reaction variables, and the variability of substrates, many parameters are known to affect the grafting of vinyl monomers to cellulose using ceric (IV) ion-initiation. General trends observed in the literature for parameters including reaction time, initiator concentration, type of acid, acid concentration, monomer concentration and substrate are briefly discussed below. Figure 13 illustrates typical curves of the grafting efficiency dependence on time, initiator concentration, acid concentration and temperature [84].

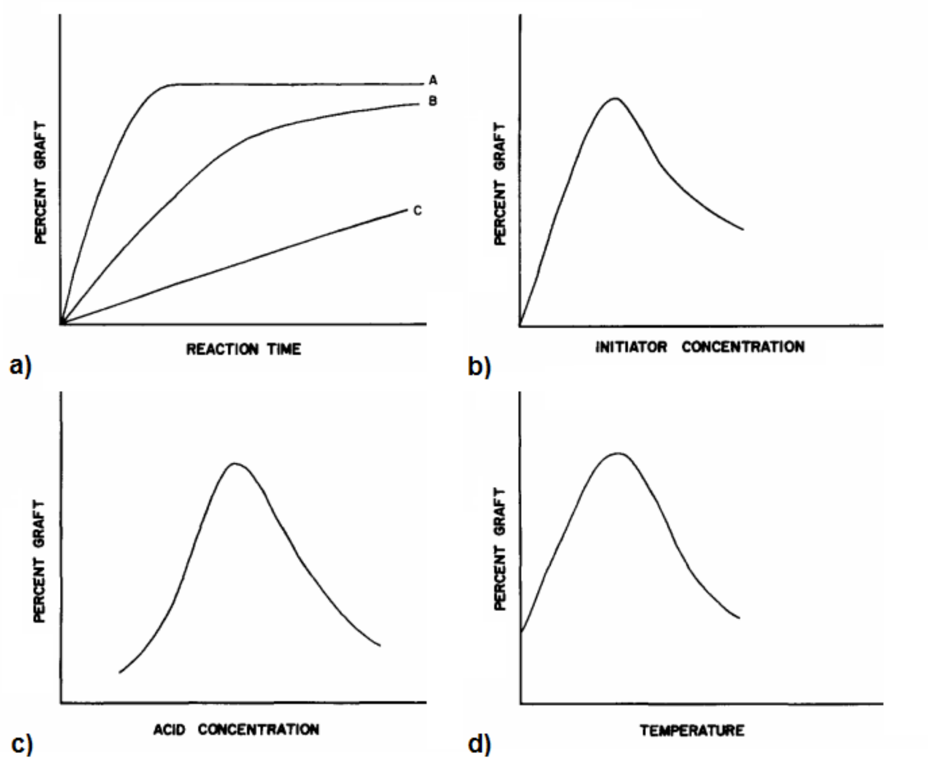

Figure 13. Typical curves of the grafting efficiency with ceric (IV) ion-initiated polymerization on cellulose as a function of (a) reaction time (b) initiator concentration (c) acid concentration (d) temperature. Figure reproduced from reference [84].

With respect to the grafting of vinyl monomers to cellulosics, many researchers have shown that the percent graft increases with time as shown in Figure 13a in one of three methods including of the grafting yield eventually leveling off with time (A), the grafting yield continuing to increase with time and eventually leveling off (B) and the grafting yield increases with reaction time (C) [87,91,92,96,97]. As the grafting efficiency increases, the rate of grafting is seen to decrease with time as there is a decrease in monomer and initiator concentration, a retardation of diffusion to the substrate with the grafted polymer chains grafted from the surface, and also a reduction in the number of available sites for grafting [84,96]. Furthermore, Figure 13b illustrates the dependence of initiator concentration on the grafting efficiency. Depending on the monomer, substrate and reaction conditions, the curve shown in Figure 13b was found to be more prevalent for ceric (IV) ammonium nitrate (CAN) than ceric (IV) ammonium sulfate (CAS). The percent grafting was found to increase with the initiator concentration until a maximum efficiency after which a decrease in percent grafting followed [87,96]. This decrease in polymer grafting with an increase in initiator concentration is suggested to be due to an increase in the rate of termination of radicals involving ceric ions (Equations 6 and 7) or due to an increase in homopolymerization [84].

The type of acid used and the concentration of acid in the reaction have been reported to affect the grafting yield. As shown in Figure 13c, it is generally suggested that an increase of acid concentration will lead to an increase in grafting as there is a decrease in the termination rate for the propagating polymer chains [104,105]. Conversely, a decrease in grafting is seen at a high acid concentration as the polymer termination rate increases and there is a reduction in the ceric-cellulose complex formation [104,105]. Furthermore, Mansour *et al*. [106] investigated the acid concentration with respect to the monomer, ceric salt and ceric ion concentration and concluded that to achieve the optimum yield, the critical factor in CAS-initiated systems was the concentration of initiator and reactivity of the monomer whereas CAN-initiated systems depended on the nitrate ion concentration.

Generally, increasing the monomer concentration increases the grafting efficiency for both CAN and CAS initiating systems for a variety of monomers and substrates

[87,91,96,104]. The monomer reactivity depends on grafting conditions as the reactivity varies for different aqueous systems and solvents and the variation of temperature also affects the monomer reactivity [107]. Moreover, the dependence of temperature on the grafting yield depends on the type of acid, the acid concentration and the monomer used. The general grafting behavior with respect to temperature is shown in Figure 13d where the change in temperature affects factors such as reactant diffusion, adsorption of the monomer to the substrate, homopolymerization and changes in the initiation, propagation and termination rates [84,87,97]. Overall, an increase in grafting with temperature corresponded to greater polymerization rates while a decrease in temperature also showed a decrease in polymerization rates.

The substrate is another important factor when considering ceric (IV)-initiated grafting of vinyl monomers to cellulosic materials. Researchers have investigated the effects of accessibility and crystallinity of the substrate and have found that an increase in accessibility and decrease in crystallinity generally lead to higher grafting yields [97,100]. Furthermore, the technique to graft monomers onto cellulosics such as treating the substrate with monomers first and then initiator or vice versa may also affect the overall grafting density. For CAN initiated systems, grafting yields were higher when the monomer was added first and the difference in yield was more pronounced at longer reaction times [87,108]. CAS initiated systems, on the other hand, showed the reverse likely because of the greater stability of CAS [84].

1.6.3 Properties of Grafted Polymers

On the basis of literature and previous works, the ceric (IV) ion-initiated graft polymerization of vinyl monomers from cellulosics generally yields a low grafting efficiency [84,109,110]. Although ceric ions sufficiently improve the number of active sites on the cellulosic backbone through the single electron transfer process, the grafted polymer molecular weights have ranged from approximately 0.03 to 11×10^5 g mol^{-1} and less than five grafted polymer chains per cellulose molecule are commonly reported [46,109,111,112]. Furthermore, the grafting reaction is understood to occur mainly in amorphous regions of cellulose, because these regions swell more in the reaction media and allow the reactants to easily diffuse through; in other words, more polymer grafting occurs in the more accessible cellulose regions [93,108,111]. By studying the morphology of polymer-grafted cellulose substrates, researchers have also reported that the grafting proceeds from the substrate surface inwards as the grafting occurs readily at the surface. X-ray analysis has shown little change in the overall crystallinity of cellulose substrates before and after the grafting-from reaction [93,113].

1.7 Research Objectives

To our knowledge, the grafting of vinyl monomers using ceric (IV) ion-initiated polymerization from cellulose nanocrystals has not been reported previously. This thesis focuses on grafting two different responsive polymers, poly(4-vinylpyridine) and poly(*N*-isopropylacrylamide), from CNCs to develop polymer-modified bio-based nanoparticles that are not only pH and temperature-responsive but also capable of showing reversible hydrophilic to hydrophobic transitions. This chemical surface modification is likely to extend the potential applications of CNCs as reinforcing agents by facilitating their incorporation into new matrix materials, in biotechnological applications, or as reversible flocculants for various industrial processes.

This thesis begins with a literature review that introduces cellulose nanocrystals, stimuli-responsive polymeric materials and the ceric (IV) ion-initiated graft polymerization mechanism. Chapter 2 provides a detailed explanation of the experimental procedures including the production of CNCs, the grafting-from CNC approach and the characterization techniques. The resultant materials, their physical and chemical properties and responsive behaviour are discussed in detail in Chapter 3. Finally, Chapter 4 summarizes the achieved results and provides recommendations for future work.

2.0 Experimental

2.1 Materials

4-vinylpyridine (4VP), *N*-Isopropylacrylamide (NIPAM), cerium (IV) ammonium nitrate (CAN), sodium chloride (NaCl), inhibitor removers, poly(4-vinylpyridine) (P4VP), M_w ~ 60000 and poly(*N*-Isopropylacrylamide) (PNIPAM), M_w ~ 19000 – 30000 were purchased from Sigma-Aldrich. Nitric acid (70%) was obtained from EMD Chemicals, polyallylamine hydrochloride (PAH, M_w = 120,000~200,000 g/mol) was purchased from Polysciences, Inc, sulfuric acid (96% ± 0.15%) was purchased from Fischer Scientific and sodium hydroxide (NaOH, 0.1 M) and hydrochloric acid (HCl, 0.1 M) were purchased from LabChem Inc.

2.2 Preparation of Cellulose Nanocrystals

Suspensions of cellulose nanocrystals were prepared by sulfuric acid hydrolysis as previously described [114]. Typically, 40 g of cotton filter aid (Whatman ashless filter aid (catalogue no. 1700025, GE Healthcare Canada, Mississauga, ON, Canada) was treated with 700 mL of 64 wt.% sulfuric acid at 45 °C for 45 min with constant stirring. Following the acid hydrolysis, the suspension was diluted 10-fold with purified Type I water with a resistivity of 18.2 MΩ cm (Barnstead NANOpure DIamond system, Thermo Scientific, Asheville, NC) to quench the reaction. The suspension was then centrifuged at 6000 rpm for 10 minutes to concentrate the cellulose, while excess water and acid were removed. The resulting precipitant was rinsed in purified water, recentrifuged and dialyzed in purified water until constant, neutral pH was achieved in the dialysis reservoir. The suspension was sonicated three times, for 15 minute intervals (Sonifier 450, Branson Ultrasonics, Danbury, CT) at 60% output while cooling in an ice bath to prevent over-heating. Dowex Marathon C hydrogen form resin (Sigma, Milwaukee, WI) was added to the cellulose suspension for three days and removed by filtering through glass microfiber filters (Whatman Grade GF/B, VWR, Chicago, IL). The resulting suspension was approximately 1% cellulose by weight and the key characteristics are labeled in the table below.

Table 2. Characteristics of sulfuric acid hydrolyzed cellulose nanocrystals.

Characteristic	
pH	3.35
AFM	122 ± 6 nm
DLS	115 ± 1 nm
Mobility	-2.36×10^{-8} m^2/Vs
Sulfur content	
Elemental Analysis	0.78%

2.3 Graft Polymerization

2.3.1 Graft Polymerization of 4-vinylpyridine

Suspensions of poly(4-vinylpyridine) grafted from cellulose nanocrystals (P4VP-*g*-CNCs) were prepared as follows. A visual schematic of the graft polymerization of 4-vinylpyridine from CNCs is shown in Figure 14. First, the 4VP monomer was passed through an inhibitor removal column. Next, 40 mL of a 1 wt.% CNC suspension, 0.75 mL of 70 wt.% HNO_3 and 1.17 mL of 4VP were added to a 50 mL round bottom flask.. Under N_2 atmosphere, the mixture was sonicated continuously at 60% output (Branson 450 sonifier) for 45 minutes in an ice bath, at which point 131 mg of CAN was dissolved in 1 mL of purified Type I water and added to the suspension. The mixture was sonicated for another 2 hours in an ice bath. The mixture was then left stirring overnight under a N_2 atmosphere. The following day, the mixture was ultra-centrifuged at 50,000 rpm for 1 hour and washed with acidic purified water (pH 2) until the UV absorbance of the supernatant at ~252 nm had decreased to 0.2–0.7 absorbance units (cerium ions strongly absorb in the UV and near UV region [84]). Sonication was applied between each centrifugation step in order to re-disperse the nanoparticles and ensure efficient removal of unreacted reagents. The P4VP-*g*-CNC suspension was filtered through glass microfiber filter paper to remove any metal particles from the sonication probe, and dialyzed against acidic water (pH 2). After dialysis, the P4VP-*g*-CNC suspension was ultrafiltrated at 3500 rpm with 100 kDa ultrafiltration tubes for 15 minutes to yield a 1 wt.% P4VP-*g*-CNC suspension, which was then stored in the refrigerator.

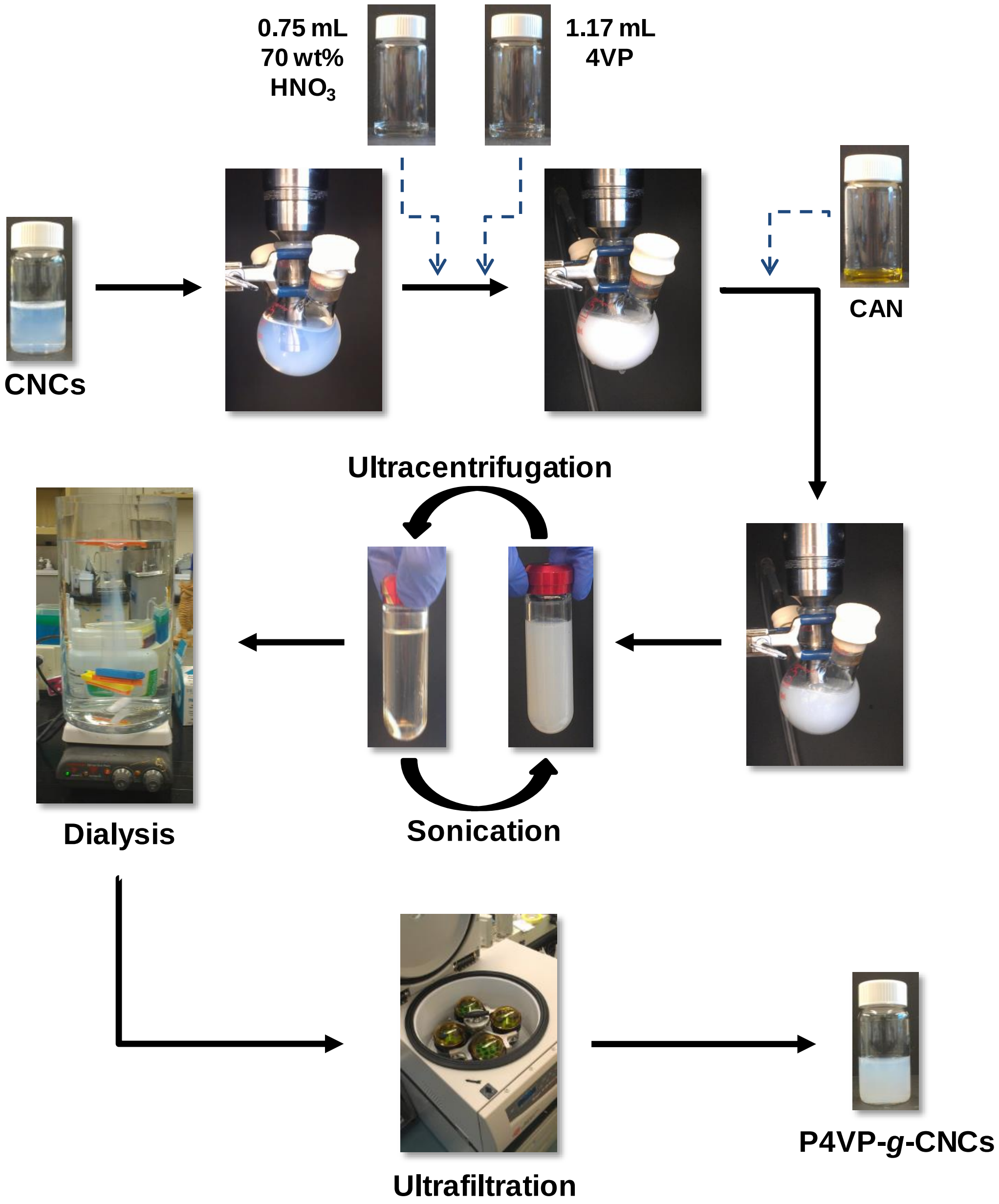

Figure 14. Schematic of the grafting polymerization of 4-vinylpyridine from CNCs.

2.3.2 Graft Polymerization of *N*-isopropylacrylamide

The graft polymerization of *N*-isopropylacrylamide from CNCs follows a similar schematic to that of the graft polymerization of 4-vinylpyridine as shown in Figure 14. First, 160 mL of a 0.25 wt. % CNC suspension, 0.75 mL of 70 wt. % HNO_3 and 1.39 g of *N*-isopropylacrylamide were added to a 500 mL round bottom flask. Under a N_2 atmosphere, the mixture was sonicated continuously in a sonicator bath (VWR Ultrasonic Cleaner) for 45 minutes in an ice bath, at which point in time, 131 mg of CAN was dissolved in 1 mL of purified water and added to the suspension. The mixture was sonicated for another 2 hours in an iced sonicator bath. The mixture was then left stirring overnight under a N_2 atmosphere. The following day, the mixture was ultra-centrifuged at 50,000 rpm for 1 hour and washed with purified water until the UV absorbance of the supernatant at ~252 nm had decreased to 0.2-0.7 absorbance units. Sonication was applied between each centrifugation step in order to re-disperse the nanoparticles and ensure efficient removal of unreacted reagents. The PNIPAM-*g*-CNC suspension was dialyzed against purified water and after dialysis, the PNIPAM-*g*-CNC suspension was ultrafiltrated in a stirred cell (Millipore, Billerica, MA) with a 30 kDa ultrafiltration membrane until there was no UV absorbance from the supernatant at ~252 nm. This process yielded a 1 wt.% PNIPAM -*g*-CNC suspension, which was then stored in the refrigerator.

2.4 Characterization Techniques

2.4.1 Fourier-Transform Infrared Spectroscopy

Freeze dried CNCs and P4VP-*g*-CNCs were incorporated into KBr pellets at approximately 1 wt.%, as was done for a neat P4VP sample. Suspensions of CNCs and PNIPAM-*g*-CNCs were also incorporated into KBr pellets at approximately 1 wt.%, as was done for a neat PNIPAM sample. FTIR spectra were recorded in transmission mode on a Nicolet 6700 FT-IR spectrometer (Thermo Scientific).

2.4.2 Elemental Analysis

Carbon, hydrogen, nitrogen and sulfur content by mass for freeze-dried CNCs and P4VP-*g*-CNCs were determined by Micro Analysis Inc. (Wilmington, DE). The samples were combusted in a pure oxygen environment where the product gases were separated and detected by thermal conductivity. Duplicates were measured for each sample and averages are reported.

2.4.3 Atomic Force Microscopy

Polished silicon wafers (Grinm Semiconductor Materials Co. Ltd, Beijing, China) were cut into 1 cm × 1 cm squares and dipped into a 0.1 wt.% PAH solution for 1 hour and rinsed in purified water to adsorb a cationic precursor layer on the substrate. The silicon wafers were then dipped into either 0.001 wt.% CNC, P4VP-*g*-CNC or PNIPAM-*g*-CNC suspensions for 1 hour and dried with compressed air. The cellulose-coated silicon wafers were imaged by AFM using a Nanoscope IIIa Multimode Scanning Probe Microscope with an E scanner (Bruker AXS, Santa Barbara, CA). The tapping mode images were collected in air with silicon cantilevers (AC 160TS, Olympus Canada Inc, Richmond Hill, ON, Canada). The dimensions of the nanocrystals were determined from AFM height images where the “width” was determined from the height values to avoid tip convolution errors. The reported error intervals represent the standard error of the average for over 100 individually measured CNCs.

2.4.4 Dynamic Light Scattering

DLS experiments were carried out with a Malvern Zetasizer Nano-S instrument (Malvern, Worcestershire, UK) with a detection angle of 173°. Suspensions of CNC and P4VP-*g*-CNC and PNIPAM-*g*-CNC with pH of 4.5, 2.5 and 5.8 respectively were filtered through a Millipore Millex-FH nylon syringe filter (0.45 μm) prior to the measurements, which were obtained at 0.05 wt.% concentrations and 25°C. The reported error intervals represent the standard error of the average of 3 measurements with 15 cycles per measurement. The effect of temperature on 0.05 wt.% suspensions of PNIPAM-*g*-CNC were collected on a temperature ramp from 20°C to 50°C with 3°C intervals and a 2 minute equilibration time between each step.

2.4.5 Electrophoretic Mobility

The electrophoretic mobility was measured using a Zeta Potential ZetaPlus Analyzer (Brookhaven, Holtsville, NY). All samples were measured at 0.25 wt.% concentrations, with 5 mM NaCl at 25 °C. All electrophoretic mobility data plotted includes error bars which represent the standard error of an average of 10 measurements with 15 cycles per measurement (in some cases the error bars are smaller than the symbols and are not necessarily visible in Figure 18).

2.4.6 Absorbance

The absorbance of PNIPAM-*g*-CNC suspensions was measured using a Cary 300 UV-Vis spectrophotometer (Agilent Technology) at a wavelength of 500 nm. The effect of temperature on 1.3 wt.% suspensions of PNIPAM-*g*-CNC were collected on a temperature ramp from 20°C to 50°C with 3°C intervals and a 5 minute equilibration time between each step. The reported error intervals represent the standard error of the average of 3 measurements.

2.4.7 Transmittance

The transmittance of all CNC and P4VP-*g*-CNC suspensions were measured using a DU®800 UV-Vis spectrophotometer (Beckman Coulter) at a wavelength of 500 nm. The concentration of the CNC and P4VP-*g*-CNC suspensions were 0.25 wt.% with a salt content of 5 mM NaCl.

2.4.8 Contact Angle

Static water contact angle measurements were conducted on a NRL contact angle goniometer, model: 100-00-115 (Ramé-hart, Succasunna, NJ) equipped with a Sanyo VC8-3512T camera. Uniform films for contact angle measurements were obtained by spin coating (Chemat Technology KW-4A, Northridge, CA) ~10 wt.% CNC, P4VP-*g*-CNC and PNIPAM-*g*-CNC suspensions onto PAH-coated Si wafers at 4000 rpm for 60 seconds followed by heat-treatment for 12 hours at 80°C. CNC and P4VP-*g*-CNC films were immersed in adjusted pH solutions of pH 2, 5 and 10 for 1 hour and then dried at 50 °C for 1 hour. Contact angles were measured with 5 μL droplets of water at pH 2, 5, and 10 on the films that had been pre-conditioned at the same pH value. Moreover, contact angles of CNC and PNIPAM-*g*-CNC films were measured with 5 μL droplets of purified Type I water (pH 5.8) at 25°C and ~40°C.

2.4.9 Ellipsometry

Film thicknesses for CNC and P4VP-*g*-CNC spin coated films were measured with an ellipsometer (Exacta 2000, Waterloo Digital Electronics, Waterloo, ON, Canada) equipped with a He-Ne laser (632.8 nm). An incident angle of 70° was used and the refractive index of cellulose was set at 1.53 [115]. Ellipsometry gave thicknesses of 66 ± 19 nm and 79 ± 7 nm, for the CNC and P4VP-*g*-CNC films, respectively.

2.4.10 Thermogravimetric Analysis

TGA measurements were performed using a thermoanalyzer (Netzsch STA-409, Burlington, MA). 20-25 mg of freeze-dried P4VP, CNCs and P4VP-*g*-CNCs were heated to 500 °C under air, with a 5 °C/min heating rate.

2.4.11 Mass Spectrometry

Two types of mass spectrometry were used to analyze P4VP grafted from CNCs: (1) laser desorption/ionization time-of-flight mass spectrometry (LDI-TOF MS) was conducted on the Micromass MALDI MicroMX spectrometer (Waters, Milford, MA) in linear mode from dried nanoparticles suspension samples without an ionizing matrix and (2) direct sample analysis time-of-flight mass spectrometry (DSA-TOF MS) was conducted on the AxION DSA System (Perklin Elmer, Waltham, MA) by applying 10 μL of each sample to the DSA rail mesh holder.

2.4.12 Optical Microscopy

Photomicrographs of P4VP-*g*-CNC suspensions were taken with a polarized light microscope (Olympus BX51) equipped with a QImaging Retiga-EXi camera. A few drops of P4VP-*g*-CNCs were placed on a standard glass microscope slide and covered with a cover slip. Pictures were taken as the P4VP-*g*-CNCs evaporated from the edges of the slide.

2.4.13 Rheology

Viscosity measurements of CNC and PNIPAM-*g*-CNC suspensions were carried out on a STRESSTECH HR Rheometer (ATS RheoSystems, Bordentown, NJ). Coaxial cylinder geometry was used at a constant shear rate of 40 s^{-1}. The effect of temperature on 2.3 wt.% suspensions of PNIPAM-*g*-CNC were collected on a temperature ramp from 20°C to 50°C with 3°C intervals and a 5 minute equilibration time between each step. The reported error intervals represent the standard error of the average of 4 measurements.

3.0 Results and Discussion

3.1 Ceric (IV) Graft Polymerization of 4-Vinylpyridine

3.1.1 Responsive Poly(4-vinylpyridine)-Grafted CNCs

P4VP-*g*-CNCs were prepared using a surface-initiated grafting-from reaction with ceric (IV) ammonium nitrate. This one-pot, water-based synthetic route is illustrated in Figure 15. The P4VP-*g*-CNC suspensions were purified by centrifugation, dialysis and ultrafiltration prior to all analyses in order to remove any unbound homopolymer and to ensure that the detected polymeric fragments were bound to the CNC surfaces which were characterized previously (Table 2). The final pH of the P4VP-*g*-CNC suspension was approximately 2.5 and showed no visible sedimentation suggesting that a stable aqueous suspension was obtained under acidic conditions. Furthermore, the presence of P4VP was confirmed on the surface of the cellulose nanocrystals by FTIR spectroscopy by comparing the spectra of pure P4VP, CNCs and P4VP-*g*-CNCs, as shown in the Figure 16. The transmittance bands at 1405, 1456, 1506 and 1556 cm^{-1} observed in P4VP-*g*-CNCs (Figure 16c) are characteristic to the stretching of the C–N and C–C bonds of P4VP (Figure 16a). This result confirms the presence of P4VP on the surface of P4VP-*g*-CNCs but does not confirm that the polymer is covalently bound to the CNCs.

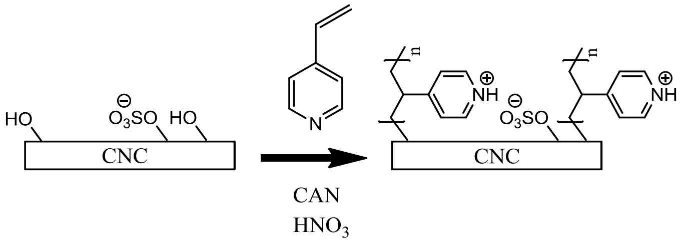

Figure 15. The graft polymerization of poly(4-vinylpyridine) with ceric (IV) ammonium nitrate (CAN) initiator from the surface of sulfuric acid-hydrolyzed cellulose nanocrystals.

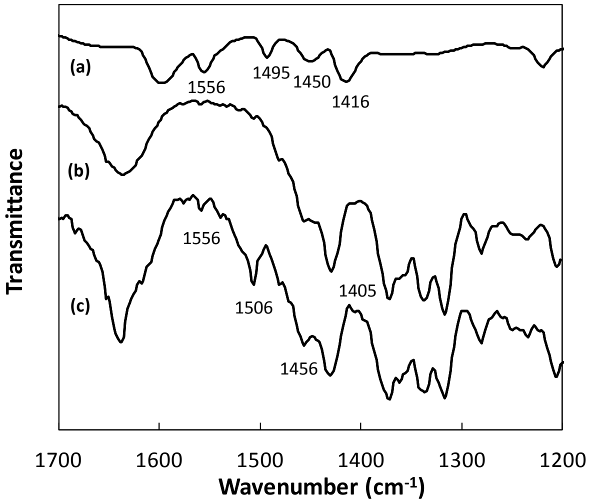

Figure 16. FTIR spectra of (a) P4VP, (b) unmodified CNCs, and (c) P4VP-*g*-CNCs.

P4VP is a weak polyelectrolyte with a pK_a ≈ 5 [116,117]. At pH > 5, P4VP becomes hydrophobic and precipitates from aqueous solution due to the deprotonation of the pyridyl group [65,66]. Suspensions of P4VP-*g*-CNCs also flocculate above pH 5, as shown macroscopically in Figure 17. Initially, both the unmodified and modified CNC samples appear stable as a function of pH (Figs. 17a and 17c). After 1 hour, the unmodified CNC suspensions remain insensitive to pH (Fig. 17b) while to the contrary, the P4VP-*g*-CNCs settle to the bottom of the vials for pH > 5 conditions (Fig. 17d). The flocculation observed in the P4VP-*g*-CNC suspensions is reversible; shifting the pH to values less than 5 returns a stable suspension since the pyridyl groups are once again protonated. Sonication will speed up the re-dispersion of P4VP-*g*-CNCs but is not required.

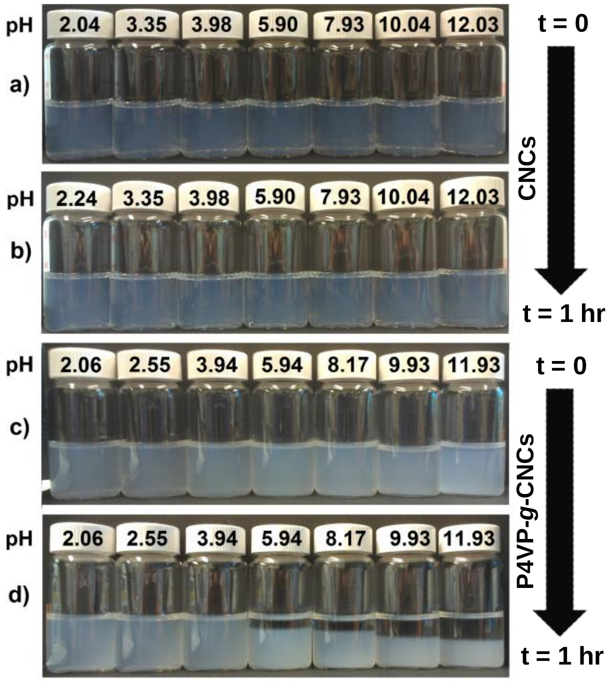

Figure 17. Photographs of (a) CNC suspensions immediately after pH adjustment and (b) 1 hour after pH adjustment; P4VP-*g*-CNC suspensions (c) immediately after pH adjustment and (d) 1 hour after pH adjustment which shows the flocculation of P4VP-*g*-CNCs above pH 5.

The pH-responsive character and surface charge of P4VP-*g*-CNCs were quantified using electrophoretic mobility measurements (Figure 18). Unmodified CNCs are negatively charged due to surface sulfate ester groups which are introduced during CNC preparation and have an electrophoretic mobility of approximately -2.5×10^{-8} m^2/Vs over the pH range studied. P4VP-*g*-CNCs, on the other hand, have a positive electrophoretic mobility at pH values less than 5 which corresponds to a cationic surface charge. At low pH values the grafted polymer chains are in an extended conformation due to the repulsive interactions between protonated pyridyl groups. At pH values above 5, the pyridyl group is deprotonated and the polymer chains collapse. When P4VP is in its collapsed uncharged state with stacked aromatic groups, P4VP-*g*-CNCs display a negative electrophoretic mobility approaching that of unmodified CNCs. The electrophoretic mobility values for P4VP-*g*-CNCs imply a stable colloidal suspension should be present due to electrostatic stabilization. This means that the flocculation observed in Figure 17 is a result of the P4VP-*g*-CNCs becoming more hydrophobic and incompatible with the aqueous environment and is not a result of charge reversal or a change in the surface charge density. Additionally, the negative surface charge above pH 5 is attributed to the CNCs' sulfate ester groups, which suggests that the polymer grafting density and the length of the P4VP polymer chains is not sufficient to completely cover, or screen, the native surface chemistry of the underlying CNCs.

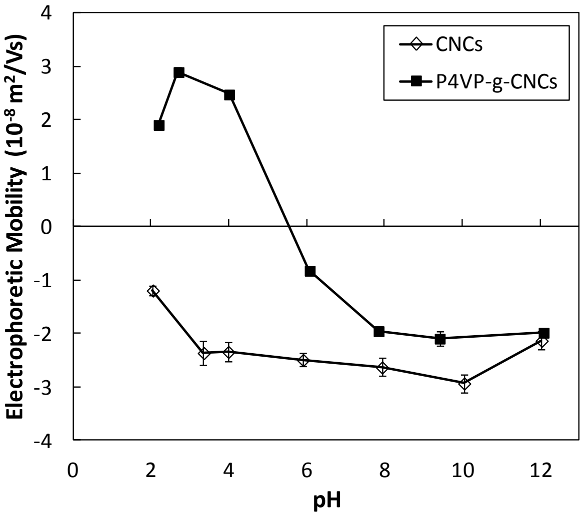

Figure 18. The effect of pH on the electrophoretic mobility of unmodified CNCs and P4VP-*g*-CNCs in aqueous suspension.

Optical transmittance for P4VP solutions, and suspensions of unmodified and polymer-grafted CNCs, was also used to characterize the material's response to pH (Figure 19). At pH values less than 4, the transmittance of the P4VP solutions is high. At pH 5, the transmittance sharply decreases due to precipitation of the hydrophobic P4VP. As shown in the inset of Figure 19, this precipitation transforms the P4VP solution from transparent to opaque due to the formation of polymer particles which scatter visible light but the polymer does not sediment over the time period of the measurement. This decline in transmittance is mirrored in the P4VP-*g*-CNC suspensions; however, the decrease is less sharp and the transition occurs over a pH range of 3–6. Conversely, the transmittance of the unmodified CNC suspension does not change over the pH range studied. The transmittance of the P4VP-*g*-CNC suspension as a function of time is presented in Figure

20 and shows that the transmittance decreases for P4VP-*g*-CNC suspensions above pH 5 over the first 300 minutes but then stabilizes as the nanoparticles flocculate and settle to the bottom of the cuvette. At pH values less than 5, the transmittance is stable as a function of time, indicating that the hydrophilic nature and repulsive interactions between cationic pyridyl groups are able to stabilize the P4VP-*g*-CNC suspensions.

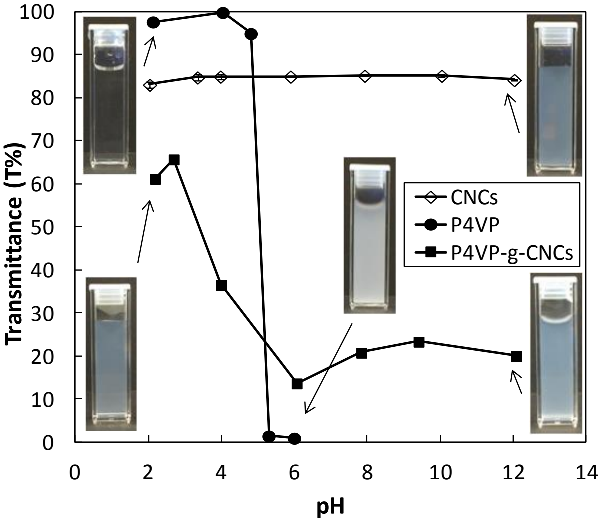

Figure 19. Transmittance of aqueous P4VP solutions, and CNCs and P4VP-*g*-CNCs suspensions. Insets show photographs of the cuvettes at the lowest and highest pH conditions tested.

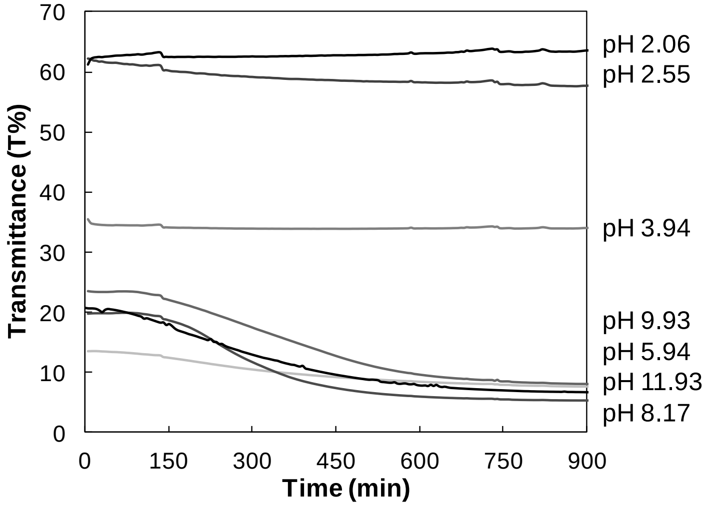

Figure 20. Transmittance of P4VP-*g*-CNC suspensions over time.

Next, the effect of suspension concentration on the responsive-nature of P4VP-*g*-CNCs was investigated (Figure 21); even at concentrations as low as 0.004 wt.%, the loss of colloidal stability for a pH 10 suspension is obvious. While the flocculation is more easily observed at high suspension concentrations, the rate of flocculation and the reversibility is not significantly concentration dependent. Generally, flocculation is visible immediately after the pH is changed and the sedimentation of particles is detected after only a few minutes (not shown).

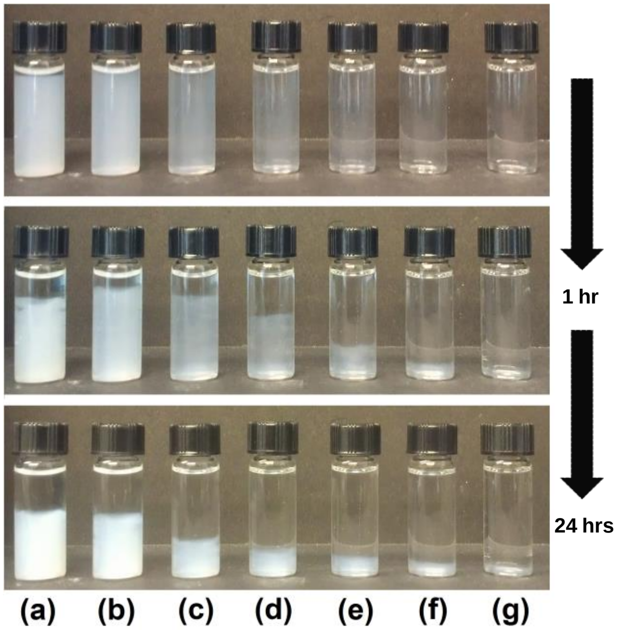

Figure 21. Photographs of P4VP-*g*-CNC suspensions (pH 10) at concentrations (a) 0.25 wt.%, (b) 0.15 wt.%, (c) 0.05 wt.%, (d) 0.025 wt.%, (e) 0.013 wt.%, (f) 0.006 wt.% and (g) 0.004 wt.% immediately after pH adjustment, 1 hour and 24 hours after pH adjustment.

Compared with other polymer-grafted responsive CNCs, the temperature-dependent CNCs with PNIPAM and Jeffamines also displayed reversible aggregation; however, the effects are not as pronounced as shown here. Nanoparticle aggregation above the LCST was measured by rheology, light scattering, and AFM but it is not evident if the responsiveness was also visible by eye or if sedimentation occurred. Interestingly, an increase in the density of grafted PNIPAM was observed to decrease the electrostatic stabilization of the CNC suspensions meaning that aggregation was a result of both the hydrophobic transition of the thermoresponsive polymer and the screening of surface charges [69]. The SI-SET-LRP reaction used by Zoppe *et al*. to modify CNCs [40,69,70], allows for the study of suspension stability and grafting yield as a function of polymer molecular weight and grafting density which could not be done with the ceric-ion initiated polymerization used here. The combination of visual inspection, electrophoretic mobility and transmittance, however, infers that the P4VP-*g*-CNCs have enough P4VP on the surface to respond in a manner predicted for P4VP while retaining some of the favourable chemical and colloidal properties of unmodified CNCs.

3.1.2 Grafting Density and Elemental Analysis

Elemental analysis supported the grafting of P4VP from the CNC surface and was used to quantify the amount of grafted polymer. Table 3 shows the atomic composition (C, H, N and S) of CNCs and P4VP-*g*-CNCs. Small amounts of sulfur from sulfate ester groups were measured in both samples and the detection of nitrogen was taken to indicate the presence of P4VP. Unmodified CNCs contained trace nitrogen and had an overall sulfur content of 0.78%, corresponding to a surface charge density of 0.34 e/nm^2 or approximately 1589 sulfate ester groups on the surface of each CNC particle. (The small decrease in %S for P4VP-*g*-CNCs compared to unmodified CNCs is merely due to the overall increase in atomic mass from grafted P4VP chains.) On the other hand, modified P4VP-*g*-CNCs had an overall nitrogen content of 0.95% corresponding to approximately 4375 pyridyl groups on each P4VP-*g*-CNC particle. This would imply a “net charge” of 2786 cationic groups per P4VP-*g*-CNC (at low pH) which concurs with the relative magnitude of the electrophoretic mobility values. 4375 pyridyl groups is approximately one 4VP repeat unit per three surface anhydroglucose units from which we can infer that the grafting density is low despite the greatly modified material properties. (Calculations for the surface charge density and the number of attached functional groups can be found in section 3.1.6. Appendix.)

Table 3. Total atomic composition by elemental analysis (EA).

	%C	%H	%N	%S
CNCs	42.37	6.29	0.03	0.78
P4VP-*g*-CNCs	44.62	6.03	0.95	0.61

Mass spectrometry (MS) was used to characterize the P4VP chains grafted from the CNC surface using two techniques: (1) laser desorption/ionization time-of-flight mass spectrometry (LDI-TOF MS) and (2) direct sample analysis-time of flight mass spectrometry (DSA-TOF MS). In accordance with the elemental analysis, both MS techniques showed small amounts of grafted polymer without elucidating the degree of grafting or the polymer molecular weight. No matrix or heat was used to collect the LDI-TOF MS spectrum of P4VP-*g*-CNCs shown in Figure 22 and as such, all peaks are attributed to P4VP released from the CNC surface. Atomic mass unit fragments which are multiples of ~105 mass units, the molecular weight of the 4VP repeat unit, were detected for up to five repeat units (indicated by the arrows with corresponding chemical structures in Figure 22). This implies that the P4VP chains grafted from the CNCs may be short, however, we did not expect to detect high molecular weight polymers with LDI-TOF MS which is designed to fragment accessible large molecules. Because CNCs are highly crystalline and rich in hydrogen bonding they do not fragment easily; the LDI-TOF MS spectrum for unmodified CNCs shows many low intensity peaks and no identifiable pattern (Figure 23). As a result, the MS peaks from CNCs are not discernible in Figure 5 with the intensity scale chosen.

Similar to the LDI-TOF MS results, the DSA-TOF MS of the unmodified CNCs gave a complex spectrum with no regular pattern. The spectrum of P4VP-*g*-CNCs did not present any sequences of repeating 4VP units, but did show a peak at the 4VP monomer mass in the total ion chromatogram (Figure 24). The total ion chromatogram, at a 106-107 mass/charge scan range detected 4VP in the P4VP-*g*-CNC suspension, and not in the CNC suspension.

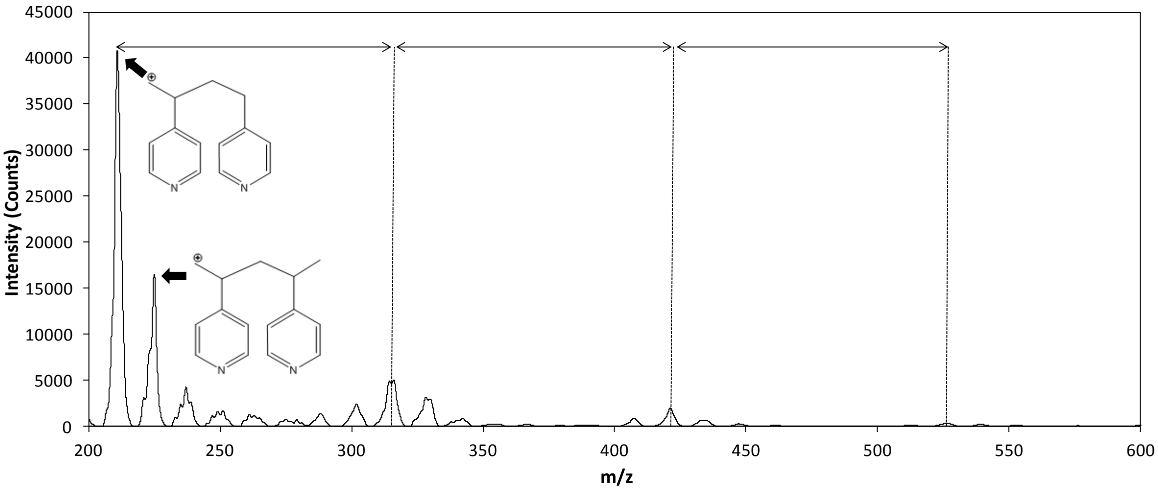

Figure 22. LDI-TOF MS spectra of P4VP-*g*-CNCs. Arrows indicate a mass difference of 105 units.

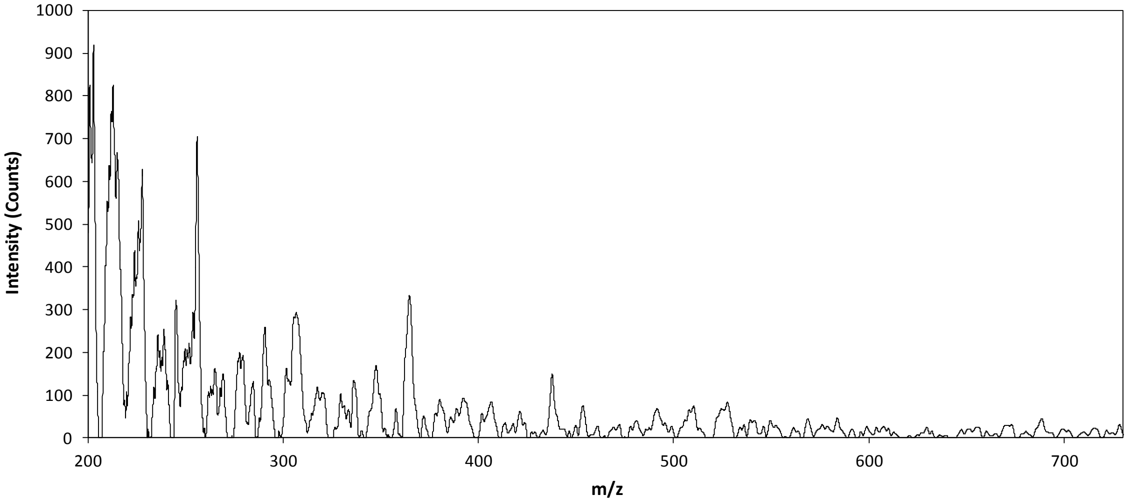

Figure 23. LDI-TOF MS spectra of a freeze-dried CNC sample.

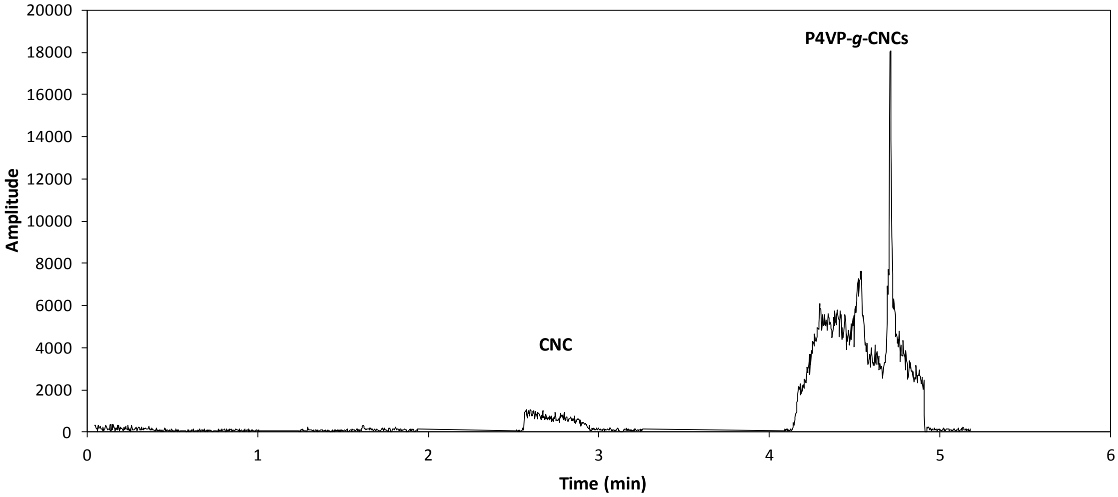

Figure 24. DSA-TOF MS spectra of CNCs and P4VP-*g*-CNCs at m/z (106:107). Vinyl pyridine monomers were detected in the P4VP-*g*-CNC suspension and not in the CNC suspension.

3.1.3 Comparison to CAN-Initiated Graft Polymerization from Other Cellulose Substrates

Two known drawbacks of grafting vinyl monomers onto cellulosics using ceric ion-initiation are believed to contribute to the low polymer content in our P4VP-*g*-CNC samples; low grafting efficiency due to homopolymerization [109] and low grafting density due to high crystallinity [84]. A number of review articles have evaluated the effect of these factors on grafting and considered other parameters such as variability of the substrate, initiator and monomer concentration, acid, reaction time, temperature, and the order in which chemicals are added [84,85,118]. Historically, cotton, wood pulp, paper, rayon, jute, ramie and cellophane have all been grafted with various vinyl monomers [85] using CAN and more recently, filter paper [119], cellulose powder [46,111,112], microcrystalline cellulose [99], and carboxymethylcellulose [120] have also proved amenable to the technique.

Previous reported grafting densities on cellulose range from 0.02 to 3 polymer grafts per cellulose chain with graft molecular weight varying between 3000 and 1.1×10^6 g/mol [46,85,111,112]. However, one specific example, which covers a range of reaction conditions, gives grafting densities of 3 to 23 grafts on a cellulose chain with a molecular weight of 2.5×10^5 g/mol [46]. These grafts have 130 to 220 repeat units per graft. In comparison, based on our yield from elemental analysis, our grafting density scales to approximately 500 4VP repeat units on a cellulose polymer chain that is 2.5×10^5 g/mol. If the repeat units were distributed evenly into three grafted chains, there would be approximately 150 repeat units per graft. (A similar argument taking into account all of the anhydroglucose units in a CNC, not just the surface units, would predict the three polymer grafts to have 56 repeat units each.) Clearly, our yield is within a reasonable range compared to previous work and is higher if we only consider the surface cellulose chains as potential grafting sites. This is a reasonable assumption given the crystallinity and intractable nature of ordered cellulose chains in CNCs.

While the grafting density is expected to be low when the crystallinity of the substrate is high, another complication, as seen here, arises; it becomes very challenging to characterize the grafted polymer chains. Previous studies have, for example, removed the grafted polymer chains by hydrolyzing the cellulose in 72 wt. % sulfuric acid for 6 hours [46,111]. As the grafting occurs mainly in the accessible amorphous regions of the cellulose, this method is able to extract the grafted polymers (and likely also produces cellulose nanocrystals!). This method is unsuitable for polymer-grafted CNCs because the initial sulfur hydrolysis has already removed the amorphous regions. Alternate chemistries to cleave covalently bound vinyl polymers from surface hydroxyl groups are not present in the literature. All in all, the combination of elemental analysis and mass spectrometry has given considerable insight into the short polymer chains and low grafting density achieved in this reaction.

3.1.4 Wettability, Morphology and Thermal Stability of PV4P-*g*-CNCs

CNC and P4VP-*g*-CNC films were prepared by spin-coating and characterized by static contact angle measurements at pH 2, 5 and 10. Prior to measurement, the films were swollen in a fixed pH solution (pH = 2, 5, or 10), and then oven-dried at 50 °C for 1 hour. Contact angle measurements were obtained by depositing a droplet of water (pH = 2, 5, or 10) onto a film which had been swollen at the corresponding pH (e.g., the contact angle of pH 2 water was measured for films swollen at pH 2). The results are presented in Table 4 and Figure 25. The contact angles of the films made from unmodified CNCs were similar at all pH values and corresponded to contact angles previously reported from spin-coated CNC films [121], whereas the P4VP-*g*-CNC surfaces exhibited a pH dependence. At pH 2, the protonated P4VP-*g*-CNC surfaces showed a more hydrophilic response in comparison to pH 5 and 10. The contact angle was expected to increase with increasing pH, as the pyridyl groups become deprotonated and collapse as shown in Figure 25a; however, as the total amount of grafted polymer was quite low, it is not surprising that the P4VP-*g*-CNC surfaces did not show very strong hydrophobic character. That said, the increase in contact angle relative to the unmodified CNCs supports the successful surface modification of CNCs with P4VP resulting in a novel material that is pH-responsive and less hydrophilic than native CNCs.

Table 4. Static contact angle measurements of films with unmodified CNCs and P4VP-*g*-CNCs at pH 2, 5 and 10.

	pH 2	pH 5	pH 10
CNC	18.9 ± 0.7°	15.1 ± 0.4°	15.7 ± 0.5°
P4VP-g-CNC	34.3 ± 0.2°	47.3 ± 0.3°	42.1 ± 0.5°

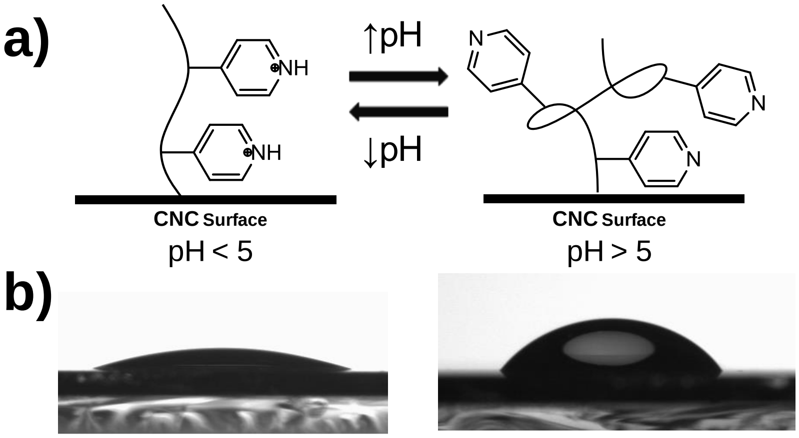

Figure 25. (a) Illustration of protonated and deprotonated pyridyl groups on P4VP-*g*-CNC surfaces at different pH (b) Contact angle of P4VP-*g*-CNC surfaces with pH 2 water (left) and pH 10 water (right).

While unmodified CNCs are notoriously difficult to disperse in organic media, P4VP-*g*-CNCs were more easily dispersed in the following solvents with short sonication treatment: water, isopropanol, dimethyl sulfoxide, dichloromethane, toluene and 1,4 dioxane (Figure 26). The P4VP-*g*-CNCs showed improved stability in all solvents (except water at high pH) when compared to the unmodified CNCs which agglomerated and quickly sedimented to the bottom of the vials in organic media. This is promising for future work which aims to evenly incorporate P4VP-*g*-CNCs into polymer matrices using solvent-borne systems.

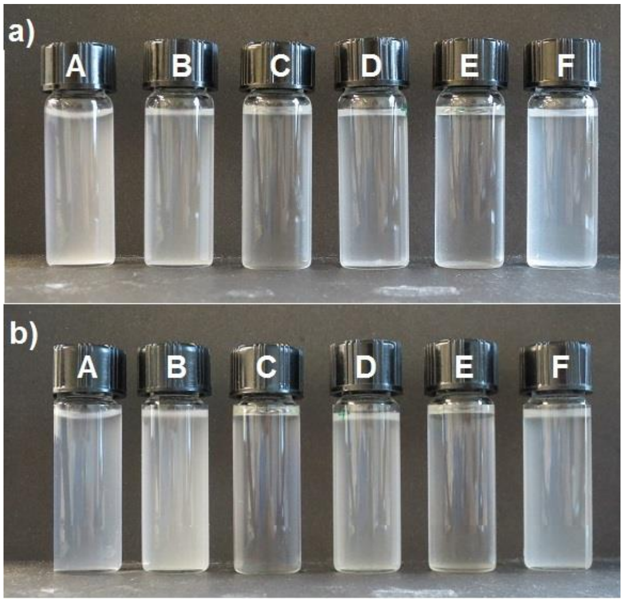

Figure 26. (a, top panel) Freeze-dried CNCs and (b, bottom panel) P4VP-*g*-CNCs dispersed in water (A), isopropanol (B), dimethyl sulfoxide (C), dichloromethane (D), toluene (E), and 1,4-dioxane (F).

Nano-scale characterization of P4VP-*g*-CNCs suspensions by AFM and DLS indicate that the polymer-grafting modification did not alter the dimensions, morphology or degree of aggregation of the starting CNCs. In order to achieve uniform surface modification and avoid particle aggregation, it was necessary to sonicate the CNC suspension during the grafting polymerization reaction. AFM height images of unmodified CNCs and P4VP-*g*-CNCs are presented in Figure 27 and show well-dispersed rod-like nanoparticles with average lengths of 122 ± 6 nm and 117 ± 8 nm and widths of 8 ± 1 nm and 8 ± 1 nm, respectively. The measured particle sizes show a monomodel size distribution (Figure 28). DLS of unmodified CNCs and P4VP-*g*-CNCs gave apparent particle sizes of 115 ± 1 nm and 95 ± 5 nm, respectively. The particle size distributions for both CNC and P4VP-*g*-CNC suspensions were monomodal, confirming the absence of aggregation in the samples. Since the DLS technique is designed to calculate the hydrodynamic diameter of spherical particles from the Stokes-Einstein equation, the results obtained are considered to be an estimate of the particle size and do not represent the actual dimensions of the rod-like nanoparticles. While DLS is useful for a quick comparison of samples, AFM was conducted to accurately measure the particle sizes.

If the grafting-from polymerization with CAN was carried out without sonication, hydrogel-like aggregates were formed. This was likely due to a combination of (i) CNC agglomeration under the reaction conditions used, (ii) CNC aggregation between CNC particles with surface radical groups and (iii) polymer bridging interactions between CNCs which arise as P4VP is polymerized from the surface. We have observed that both a probe sonicator and sonicator bath are sufficient to avoid this aggregation.

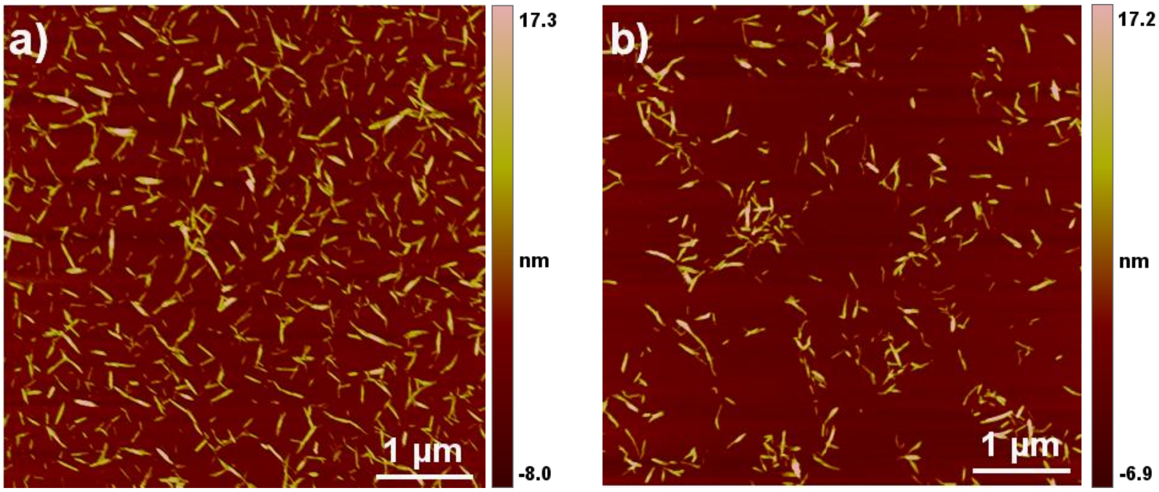

Figure 27. AFM height images of (a) unmodified CNCs and (b) modified P4VP-*g*-CNCs.

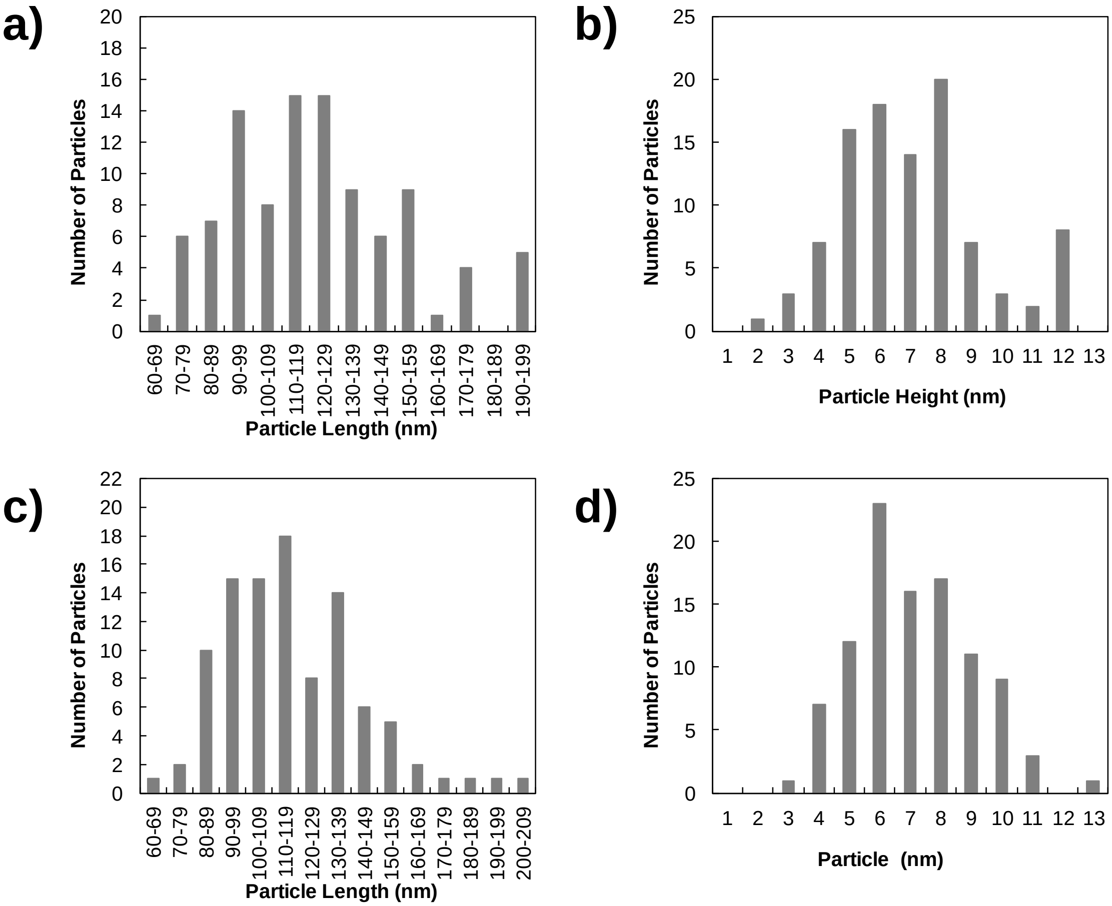

Figure 28. CNC and P4VP-*g*-CNC particle size distribution from analyses of AFM height images: (a) length of unmodified CNCs and (b) height of unmodified CNCs and (c) length of P4VP-*g*-CNCs and (d) height of P4VP-*g*-CNCs.

Enhanced thermal stability of P4VP-*g*-CNCs was observed from TGA analysis (Figure 29) also supports the success of the grafting-from polymerization on CNCs. This is strong evidence that the P4VP is covalently attached to the CNCs as only one peak is evident in the TGA and the derivate thermogravimetric analysis curves for P4VP-*g*-CNCs (Figure 29 and 30). The onset of thermal degradation has been shifted from 208°C for unmodified CNCs to 267°C for the P4VP-*g*-CNCs. As expected, the thermal stability of P4VP-*g*-CNCs is intermediate between unmodified CNCs and pure P4VP.

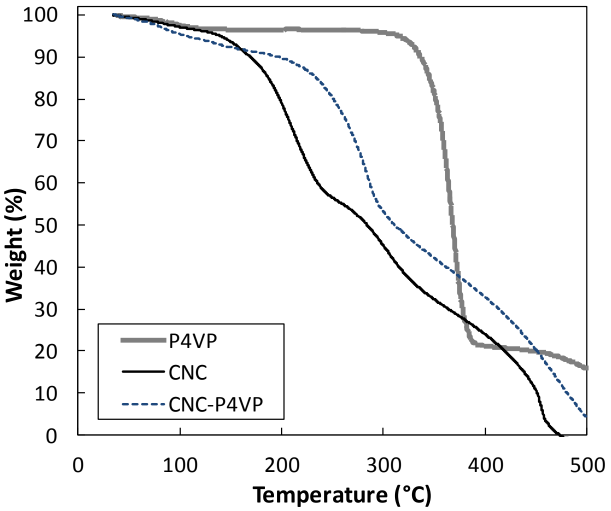

Figure 29. Thermogravimetric curves of P4VP, unmodified CNCs and P4VP-*g*-CNCs.

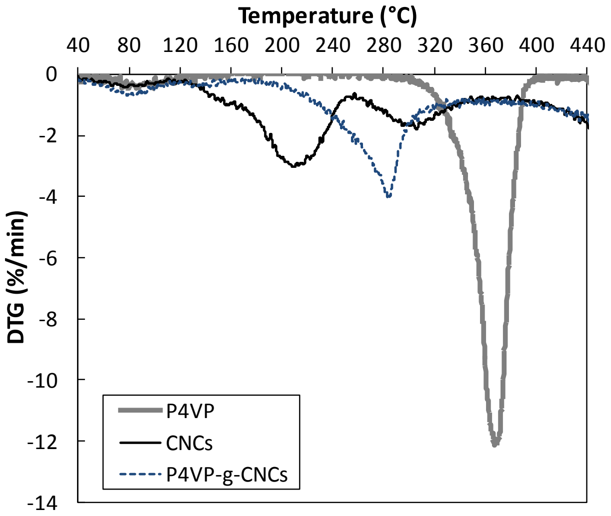

Figure 30. Derivate thermogravimetric analysis curves (DTG) curves of P4VP, unmodified CNCs and P4VP-*g*-CNCs.

P4VP-*g*-CNC suspensions displayed a thread-like nematic liquid crystal texture when observed under polarized light microscopy (Figure 31) [122]. The chiral nematic liquid crystal phase normally observed for unmodified CNCs [2] was not detected indicating a change in the self-assembly properties of the polymer-grafted CNCs. This may be due to partial screening of native CNC surface charges and particle geometry by the P4VP polymer chains, leading to a loss of chirality. While the liquid crystalline properties for most polymer-grafted CNCs have not been investigated, CNCs with PEG [18,71], poly(N,N-dimethylaminoethyl methacrylate) [123], and polystyrene [42] have shown chiral nematic liquid crystal textures.

Finally, the qualitative gelation behaviour of P4VP-*g*-CNCs were unique; the onset of gelation occurred at lower concentrations than for unmodified CNCs and P4VP-*g*-CNCs were found to exhibit shear thinning behavior at concentrations above 10 wt.%.

The P4VP-*g*-CNC gels appear stable and unmoving when a sample vial is slowly inverted but flow when the vial is agitated (Figure 32). Our unmodified CNCs prepared by sulfuric acid hydrolysis do not show this shear-thinning behaviour at similar concentrations. Since gelation also corresponds to a destabilization of the colloidal suspension, there are many ways to induce gel formation in CNC suspensions. Processes such as exchanging the counterions associated with the charged ester groups from monovalent to divalent ions,[31] increasing the ionic strength [73], functionalizing the surface of the CNCs with cationic hydroxypropyltrimethylammonium chloride [34], carboxylic acid or amine moieties [49], along with evaporating water from aqueous glycerol suspensions of CNCs [74], have all lead to similar gelation properties.

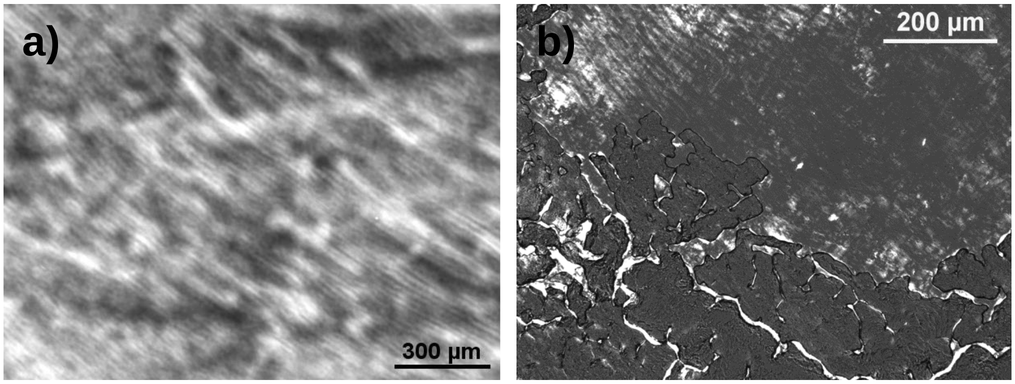

Figure 31. Polarized light microscopy images of (a) unmodified CNCs which form a chiral nematic liquid crystal texture above a critical concentration and (b) a P4VP-*g*-CNCs suspension showing a nematic thread-like liquid crystal texture.

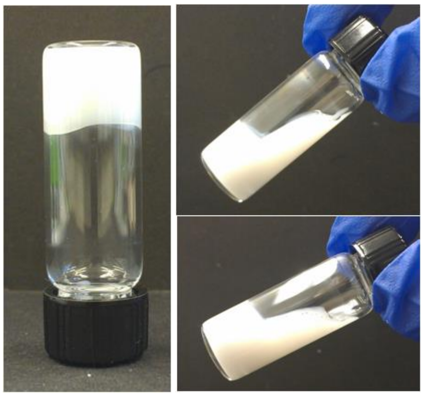

Figure 32. Photographs of P4VP-*g*-CNC gels exhibiting shear thinning behaviour.

3.1.5 Summary

pH-responsive CNCs were successfully prepared by grafting poly(4-vinylpyridine) from CNC surface hydroxyl groups via ceric ion-initiated polymerization in water. Above pH 5, P4VP-*g*-CNCs flocculated and sedimented from suspension due to the deprotonation of poly(4-vinylpyridine). Colloidally stable suspensions were easily regenerated by decreasing the pH. Extensive characterization confirmed the grafting reaction was effective and gave a reasonable grafting density compared to previously published work on grafting vinyl monomers from other cellulose substrates. Approximately one 4-vinylpyridine repeat unit was detected for every three surface anhydroglucose units or 4375 4-vinylpyridine repeat units per cellulose nanocrystal.

In this case specifically, the pH-responsive character of the novel P4VP-*g*-CNC hybrid material allows us to tune the nanoparticle surface charge from cationic to anionic, the wettability from hydrophilic to hydrophobic, and the suspension stability from stable to flocculated, in a reversible manner. P4VP-*g*-CNCs are more thermally stable than native CNCs, self-assemble into a nematic liquid crystal, and form gels with shear-thinning behaviour at high concentrations. These controlled properties offer new potential to achieve a uniform dispersion of CNCs in hydrophobic polymer matrices for reinforcing applications, and opens up a range of opportunities for pH-responsive CNC-based materials.

3.1.6 Appendix

Elemental Analysis Calculations:

The grafting density of both sulfate ester groups and poly(4-vinylpyridine) repeat units was calculated from the elemental analysis results in Table 2 combined with literature values from X-ray diffraction data of cellulose [124], with the assumptions listed below.

Assumption 1: CNCs are square prisms.

Assumption 2: The ends of CNCs are non-reactive.

Assumption 3: The cellulose unit cell contains four anhydroglucose units (AGUs). These four AGUs are all exposed on the surface of the unit cell.

Assumption 4: Sulfate ester groups from the acid hydrolysis preparation of CNCs are not affected during the graft polymerization reaction.

Table 5. Calculation of surface grafting density of sulfate ester groups on unmodified CNCs.

		CNCs	Cellulose unit cell [124]
Length	[nm]	122	1.08
Width	[nm]	7.57	0.820
Total Volume	[nm^3]	6984	0.692 (calc.)
Number of cellulose unit cells per CNC		10092	
Number of total AGUs per CNC		40368	
Active surface area	[nm^2]	3689	0.889 (calc.)
Number of surface cellulose unit cells per CNC		3781	
Number of surface AGUs per CNC		15123	
Density of CNC[2]	[g/nm^3]	1.61E-21	
Weight of 1 CNC particle	[g]	1.12E-17	
<u>Sulfur content</u>	[S wt.%]	0.78	
	[mol S/g cellulose]	2.44E-4	
Weight of sulfur	[atoms S/g cellulose]	1.47E+20	
Number of S atoms per CNC particle		1650	
Number of surface AGUs per CNC		15123	
Number of surface AGUs per S *(sulfate ester group)*		**9.16**	

Table 6. Calculation of grafting density of 4-vinylpyridine repeat units on modified CNCs.

		P4VP-*g*-CNCs	Cellulose unit cell [124]
Length	[nm]	117	1.08
Width	[nm]	7.67	0.820
Total Volume	[nm^3]	6907	0.692 (calc.)
Number of cellulose unit cells per CNC		9982	
Number of total AGUs per CNC		39927	
Active surface area	[nm^2]	3601	0.889 (calc.)
Number of surface cellulose unit cells per CNC		3695	
Number of surface AGUs per CNC		14782	
Density of CNC[2]	[g/nm^3]	1.61E-21	
Weight of 1 CNC particle	[g]	1.11E-17	
Nitrogen content	[N wt.%]	0.95	
	[mol N/g cellulose]	6.79E-4	
Weight of nitrogen	[atoms S/g cellulose]	4.09E+20	
Number of N atoms per CNC particle		4544	
Number of total AGUs per CNC		39927	
Number of total AGUs per N *(4VP repeat unit)*		**8.79**	
Number of surface AGUs per CNC		13131	
Number of surface AGUs per N *(4VP repeat unit)*		**2.89**	

3.2 Ceric (IV) Graft Polymerization of *N*-isopropylacrylamide

3.2.1 Responsive Poly(*N*-isopropylacrylamide)-Grafted CNCs

PNIPAM-*g*-CNCs were prepared using a surface-initiated grafting-from reaction with CAN. The PNIPAM-*g*-CNC suspensions were purified by centrifugation, dialysis and ultrafiltration prior to all analyses in order to remove any unbound homopolymer and to ensure that the detected polymer moieties were bound to the CNCs. The final pH of the PNIPAM-*g*-CNC suspension was 5.8 and showed no visible sedimentation suggesting that a stable aqueous suspension was obtained. The presence of PNIPAM was confirmed on the surface of the cellulose nanocrystals by FTIR spectroscopy by comparing the spectra of pure PNIPAM, CNCs and PNIPAM-*g*-CNCs, as shown in Figure 34. The transmittance bands at 1550 and 1645 cm^{-1} observed in PNIPAM -*g*-CNCs (Figure 34c) are characteristic to the amine stretch and amine bend of PNIPAM (Figure 34a) [40,125]. This result confirms the presence of PNIPAM on the surface of PNIPAM -*g*-CNCs but does not confirm that the polymer is covalently bound to the CNCs.

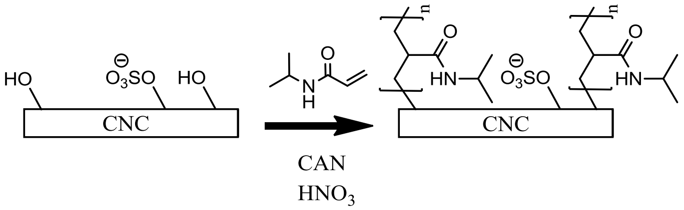

Figure 33. The graft polymerization of poly(*N*-isopropylacrylamide) with ceric (IV) ammonium nitrate (CAN) initiator from the surface of sulfuric acid-hydrolyzed cellulose nanocrystals.

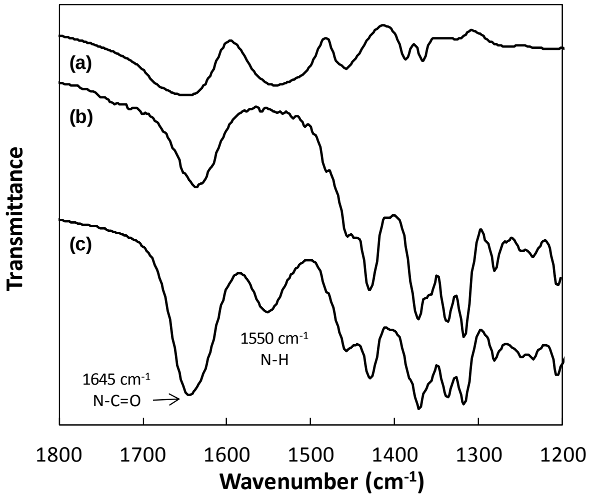

Figure 34. FTIR spectra of (a) PNIPAM, (b) unmodified CNCs, and (c) PNIPAM-*g*-CNCs.

PNIPAM is a non-ionic polymer with the presence of an isopropyl group on the polymer chain which gives PNIPAM its hydrophobic character [60]. When PNIPAM is dissolved in water, water reorganizes and assembles a cage-like structure around the isopropyl groups [126]. PNIPAM is one of the most studied thermoresponsive polymers and possess a lower critical solution temperature (LCST) in aqueous solution of ~31°C where above this temperature, a phase separation dependent on the concentration and molecular weight occurs [127]. This involves the hydrophobic and hydrophilic domains of PNIPAM rearranging depending in the water content of the material, the surrounding media (air or liquid) and the ambient temperature. Generally above the LCST, a linear PNIPAM macromolecular chain transitions from being an extended flexible coil to collapsing to a stiff globular state [60] due to the thermal dehydrations of the polymer chain that yields an entropic gain in free energy of the system [58,69]. Matsuyama *et al.*

[128] explained the LCST of PNIPAM as the mixing entropy produced by solvation and additionally, the LCST is affected by factors such as ionic strength and pH of the solution or aqueous suspension [129,130].

The reversible thermo-responsive character of PNIPAM-*g*-CNCs was evaluated by measuring the effect of temperature on the DLS hydrodynamic diameter of a 0.05 wt. % PNIPAM-*g*-CNC suspension as shown in Figure 35. When the temperature was increased from 20°C to 30°C, the apparent hydrodynamic diameter was relatively constant at approximately 87 nm. An increase in the hydrodynamic diameter was observed from 30°C to 40°C, showing a possible explanation of the formation of agglomerates within the suspension. Cooling the suspension back to 20°C resulted in the hydrodynamic diameter decreasing and returning to a similar value that was observed before heating. This result confirms the thermosensitive character of PNIPAM-*g*-CNC and shows that the temperature-induced aggregation is reversible with a slight 3°C hysteresis when cooling down.

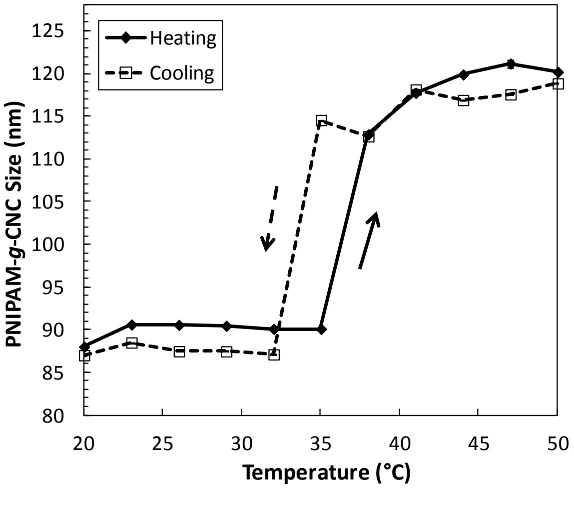

Figure 35. Hydrodynamic diameter as a function of temperature for PNIPAM-*g*-CNCs.

The thermoresponsiveness of unmodified CNCs and PNIPAM-*g*-CNCs in aqueous suspensions were analyzed by ultraviolet-visible spectroscopy at a wavelength of 500 nm. Unmodified CNCs showed no change in absorbance for the temperature range of 20 to 50°C tested (not shown) demonstrating that CNCs were not responsive to temperature. On the other hand, Figure 36 illustrates the absorbance versus temperature of PNIPAM-*g*-CNCs which shows a clear increase in the optical density at a temperature above the LCST of PNIPAM. This is also in good agreement with the particle size increase shown in Figure 35. Photographs in Figure 36 also show PNIPAM-*g*-CNC suspensions observed at a low and high temperature where the suspension turns from being clear into a turbid milky suspension.

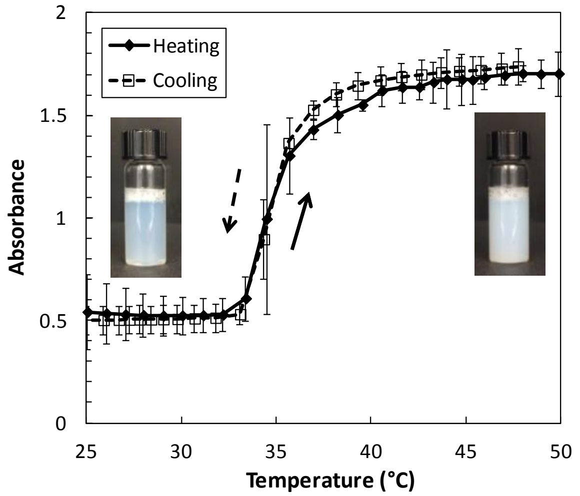

Figure 36. Absorbance at 500 nm versus temperature of a 1.2 wt. % PNIPAM-*g*-CNC suspension.

Further evidence of the aggregation and thermal responsiveness of PNIPAM-*g*-CNC suspensions were analyzed by viscosity measurements. Aqueous suspensions of

CNCs and PNIPAM-*g*-CNCs at 2.3 wt. % were equilibrated at 20°C on an ATS RheoSystems rheometer with coaxial cylinder geometry. The viscosity was monitored over a temperature range of 20°C to 50°C at a constant shear rate of 40 s^{-1} and the results are summarized in Figure 37. Generally, the viscosity of colloidal suspensions in Newtonian fluids decreases with increasing temperature as explained by the Arrhenius relationship of molecular kinetics [131] and this is reflected in unmodified CNC suspensions as shown in Figure 37. PNIPAM-*g*-CNC suspensions on the other hand showed a significant increase in viscosity as the temperature approached the LCST of the grafted PNIPAM polymer. Below 35°C, the viscosity of the PNIPAM-*g*-CNC suspension showed a viscosity similar to that of unmodified CNC suspensions while the viscosity increased as the LCST was approached. These results are also in agreement with the work performed by Zoppe *et al.* [69] who used viscometry to indicate the thermo responsiveness of PNIPAM grafted from CNCs via SI-SET-LRP.

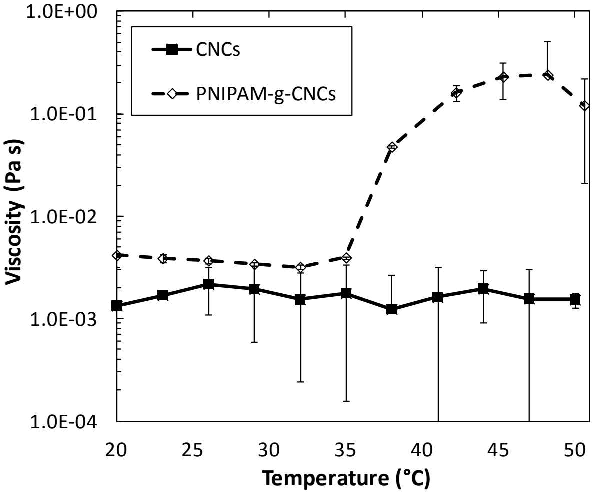

Figure 37. Viscosity of 2.3 wt. % suspensions of unmodified CNCs and PNIPAM-*g*-CNCs at different temperatures.

The reversibility of PNIPAM-*g*-CNC aggregation and thermo responsiveness is shown in Figure 35 while heating the suspension from 20 to 50°C and then cooling back to the initial temperature. To the contrary, the PNIPAM-*g*-CNC suspension only exhibited a partially recoverable thermo-responsive behavior with respect to viscosity (Figure 38). Upon cooling, the viscosity did not revert back completely to the initial value, suggesting the presence of some agglomerates. However, sonicating the suspension did help redisperse the PNIPAM-*g*-CNCs and the viscosity reverted back to its initial value. Photographs in Figure 38 also show the change in suspension flowability with temperature. At a temperature of 20°C, the suspension has a viscosity similar to that of water while as the LCST is approached, the suspension gels due to the dehydration of the grafted polymer brushes on the CNCs which decreases the stability of the suspension.

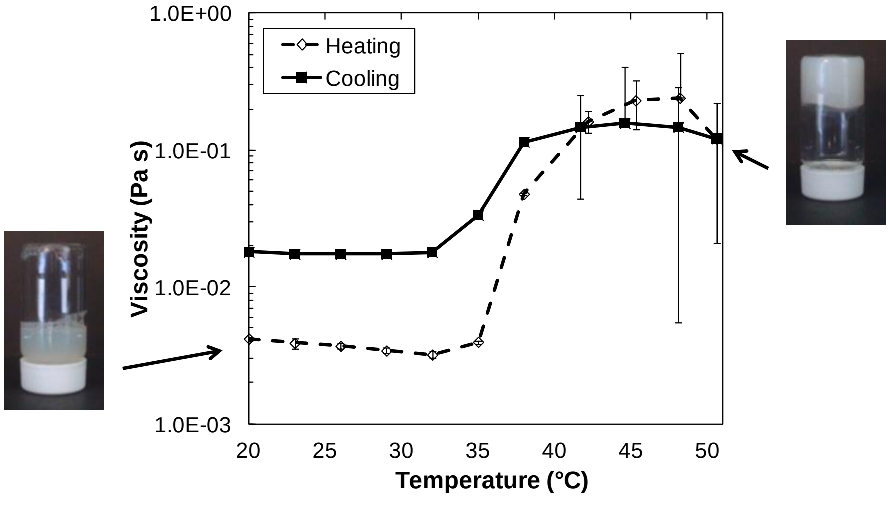

Figure 38. Viscosity of a 2.3 wt. % suspension of PNIPAM-*g*-CNC in a heating and cooling process.

3.2.2 Wettability, Morphology and Surface Charge of PNIPAM-*g*-CNCs

CNC and PNIPAM-*g*-CNC films were prepared by spin-coating and characterized by static contact angle measurements at temperatures of ca. 25°C and 40°C. Prior to measurements, the films were equilibrated at a fixed temperature and then contact angle measurements were obtained by depositing a droplet of purified Type I water (pH 5.8) onto the film. The results are presented in Table 7. The contact angles of the films made from unmodified CNCs were similar at both temperatures whereas the PNIPAM-*g*-CNC surfaces exhibited a temperature dependence. At 25°C, the PNIPAM-*g*-CNC surfaces showed a more hydrophilic response in comparison to 40°C, however, the difference was not statistically significant. The contact angle was expected to increase with increasing temperature as the extended flexible coils collapse to a compact and stiff globular state. However, as the grafting density is assumed to be quite low, based on the results previously reported for P4VP-*g*-CNCs, it is not surprising that the PNIPAM-*g*-CNC surfaces did not show very strong hydrophobic character. The increase in contact angle relative to the unmodified CNCs supports the successful surface modification of CNCs with PNIPAM resulting in a novel material that is temperature-responsive and less hydrophilic than native CNCs.

Table 7. Static contact angle measurements of films with unmodified CNCs and PNIPAM-*g*-CNCs at 25°C and 40°C.

	25°C	40 °C
CNC	19.4 ± 4.6°	16.3 ± 7.4°
PNIPAM-*g*-CNCs	19.2 ± 27.6°	47.3 ± 7.07°

Nano-scale characterization of PNIPAM-*g*-CNCs by AFM and DLS indicate that the polymer-grafting modification did not alter the dimensions, morphology or degree of aggregation of the starting CNCs. As explained previously, DLS is used as a quick comparison of samples and does not represent the actual dimensions of the rod-like nanoparticles. DLS gave apparent particle sizes of 115 ± 1 nm and 156 ± 7 nm for unmodified CNC and PNIPAM-*g*-CNCs, respectively. A monomodal particle size distribution was evident for both suspensions confirming the absence of aggregation in the samples. Moreover, AFM height images of the unmodified CNCs were previously presented in Figure 27a with the particle size distributions shown in Figure 28a and b. Figure 39 presents an AFM height image and the particle size distribution of PNIPAM-*g*-CNCs. The AFM images of unmodified and modified CNCs show well-dispersed rod-like nanoparticles with average lengths of 122 ± 6 nm and 116 ± 6 nm and widths of 6 ± 1 nm and 6 ± 1 nm, respectively. A monomodel size distribution was also evident for both unmodified CNCs and PNIPAM-*g*-CNCs.

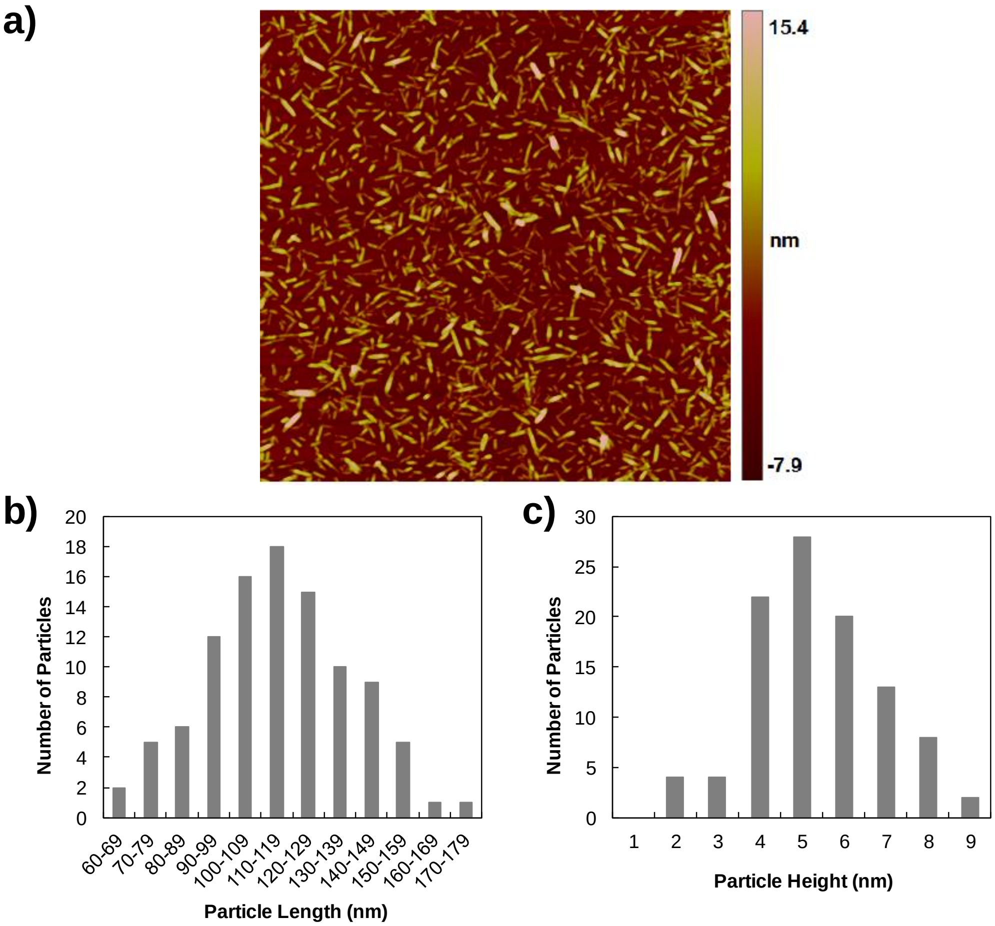

Figure 39. (a) AFM height image of PNIPAM-*g*-CNCs. PNIPAM-*g*-CNC particle size distribution from analyses of AFM height images: (b) length of PNIPAM-*g*-CNCs and (c) height of PNIPAM-*g*-CNCs.

The surface charge of CNCs and PNIPAM-*g*-CNCs were quantified by electrophoretic mobility measurements. Unmodified CNCs have an electrophoretic mobility of approximately -2.5×10^{-8} m^2/Vs, as shown previously in Figure 18, due to the negative surface sulfate ester groups introduced during CNC preparation. PNIPAM-*g*-CNCs, on the other hand also have an electrophoretic mobility of -2.5×10^{-8} m^2/Vs at pH 5.8. This result confirms that the sulfate ester groups are preserved during the grafting reaction and a stable colloidal suspension is present due to electrostatic stabilization. This is also expected as the ceric (IV) ion-initiated graft polymerization generally initiates free radicals from CNC surface hydroxyl groups and the grafted polymer PNIPAM is a non-ionic polymer.

3.2.3 Summary

Temperature-responsive CNCs were successfully prepared by grafting poly(*N*-isopropylacrylamide) from CNC via ceric ion-initiated polymerization in water. Above the LCST of PNIPAM, PNIPAM-*g*-CNCs agglomerated in suspension and gelled, depending on the concentration of the suspension. Colloidally stable suspensions were easily regenerated by decreasing the temperature and extensive characterization confirmed the grafting reaction was effective. Overall, this aqueous reaction is an easy way to modify individual nanoparticles and achieve reproducible and uniform material properties.

In this case specifically, the temperature-responsive character of the novel PNIPAM-*g*-CNC hybrid material allows us to reversibly tune the wettability and the suspension stability from stable to agglomerated or gelled. As in the case of P4VP-*g*-CNCs, these tailorable properties offer new potential to achieve a uniform dispersion of CNCs in various hydrophobic materials and may open up a new range of applications for responsive CNC-based materials.

4.0 Conclusions and Recommendations

4.1 Conclusions

Cellulose nanocrystals responsive to pH and temperature were successful synthesized by grafting 4-vinylpyridine and *N*-isopropylacrylamide from CNCs via ceric (IV) ion-initiated polymerization in water. The resulting P4VP-*g*-CNC and PNIPAM-*g*-CNC suspensions show reversible hydrophilic to hydrophobic responses with changes in pH and temperature, respectively. FTIR, mass spectrometry, elemental analysis, electrophoretic mobility, UV spectroscopy, contact angle measurements and thermal analysis confirmed the success of the reaction and determined that P4VP-*g*-CNCs and PNIPAM-*g*-CNCs have new surface chemistries.

The novel P4VP-*g*-CNC hybrid material allows us to tune the nanoparticle wettability, the surface charge from cationic to anionic, and the suspension stability from stable to flocculated, in a reversible manner by changing the pH. Above pH 5, P4VP-*g*-CNCs quickly flocculated and sedimented from suspension due to the deprotonation of poly(4-vinylpyridine). On the other hand, the PNIPAM-*g*-CNC hybrid material allows us to reversibly control the wettability and the suspension stability from stable to agglomerated or gelled, depending on the suspension concentration, by increasing the temperature above the LCST of PNIPAM.

This is the first report of using ceric ion-initiated polymerization with cellulose nanocrystals and we have found that this aqueous reaction is an easy way to modify individual nanoparticles and achieve reproducible and uniform material properties.

Importantly, CNCs remained dispersed during the grafting-from reaction because of the constant sonication treatment and the surface modification did not induce particle aggregation. The approach presented here can likely be extended to other water soluble vinyl monomers to give CNCs with controlled interfacial compatibility and functionality.

Finally, controlled stability and wettability of P4VP-*g*-CNCs and PNIPAM-*g*-CNCs is advantageous both in composite design, where cellulose nanocrystals generally have limited dispersibility in non-polar matrices. The responsive nature of these novel nanoparticles may offer new applications for CNCs in biomedical devices, as clarifying agents, and in industrial separation processes.

4.2 Recommendations

The ceric (IV) ion-initiated graft polymerization of 4-vinylpyridine and *N*-isopropylacrylamide from CNCs is a simple way to modify individual nanoparticles and achieve reproducible and uniform material properties. Even though the surface modified P4VP-*g*-CNC and PNIPAM-*g*-CNC suspensions show reversible hydrophilic to "much less hydrophilic" responses which are visible by eye, the contact angle measurements did not show a very strong hydrophobic character (i.e., contact angle did not surpass 90^o) for both P4VP-*g*-CNC and PNIPAM-*g*-CNC spin-coated surfaces. This is likely due to the fact that the grafting density is low and cellulose is a hydrophilic material. To create modified CNCs that show a stronger hydrophobic character, reaction conditions such as initiator and monomer concentration, acid, reaction time, temperature may be optimized. Extensive purification should also be performed prior to all analyses to ensure that the detected polymeric fragments are bound to the CNC surfaces and not unbound homopolymer. Furthermore, the current reaction of 0.4 g of CNCs can be scaled up. Successful P4VP-*g*-CNCs have been synthesized from a 10X scaled up protocol by running the reaction in a sonicator bath, instead of with a sonicator probe, while stirring mechanically.

Modified CNCs can be introduced as reinforcing agents to non-polar materials. As P4VP-*g*-CNCs showed improved stability in various organic solvents compared to the unmodified CNCs, introducing modified CNCs that are less hydrophilic into various polymer matrices may inhibit agglomeration and improve dispersion and thus the strength of the nanocomposites. Additionally, new applications are envisioned for the modified CNCs. The triggered response may prove useful in biomedical applications where pH or temperature switching could, for example, trigger the release of therapeutics. The reversible flocculating behaviour of P4VP-*g*-CNC suspensions at concentrations as low as 0.004 wt.% implies that the modified CNCs could be used as flocculating agents in various industries. If target binding sites were also incorporated onto the CNC surfaces, the P4VP-*g*-CNCs could be used in industrial separation processes, for example, to remove pharmaceuticals from wastewater.

5.0 References

[1] P. Tingaut, T. Zimmermann, G. Sèbe, Cellulose nanocrystals and microfibrillated cellulose as building blocks for the design of hierarchical functional materials, J. Mater. Chem. 22 (2012) 20105–20111.

[2] Y. Habibi, L.A. Lucia, O.J. Rojas, Cellulose nanocrystals: chemistry, self-assembly, and applications, Chem. Rev. 110 (2010) 3479–3500.

[3] S. Eichhorn, A. Dufresne, M. Aranguren, N. Marcovich, J. Capadona, S. Rowan, et al., Review: current international research into cellulose nanofibres and nanocomposites, Journal of Materials Science. 45 (2010) 1–33.

[4] R.J. Moon, A. Martini, J. Nairn, J. Simonsen, J. Youngblood, Cellulose nanomaterials review: structure, properties and nanocomposites, Chem. Soc. Rev. 40 (2011) 3941–3994.

[5] Y. Nishiyama, Structure and properties of the cellulose microfibril, J Wood Sci. 55 (2009) 241–249.

[6] D. Klemm, F. Kramer, S. Moritz, T. Lindström, M. Ankerfors, D. Gray, et al., Nanocelluloses: A New Family of Nature-Based Materials, Angewandte Chemie International Edition. 50 (2011) 5438–5466.

[7] M.A.S. Azizi Samir, F. Alloin, A. Dufresne, Review of Recent Research into Cellulosic Whiskers, Their Properties and Their Application in Nanocomposite Field, Biomacromolecules. 6 (2005) 612–626.

[8] B.G. Rånby, Fibrous macromolecular systems. Cellulose and muscle. The colloidal properties of cellulose micelles, Discuss. Faraday Soc. 11 (1951) 158–164.

[9] S. Beck-Candanedo, M. Roman, D.G. Gray, Effect of Reaction Conditions on the Properties and Behavior of Wood Cellulose Nanocrystal Suspensions, Biomacromolecules. 6 (2005) 1048–1054.

[10] X.M. Dong, J.-F. Revol, D.G. Gray, Effect of microcrystallite preparation conditions on the formation of colloid crystals of cellulose, Cellulose. 5 (1998) 19–32.

[11] O.A. Battista, S. Coppick, J.A. Howsmon, F.F. Morehead, W.A. Sisson, Level-Off Degree of Polymerization, Ind. Eng. Chem. 48 (1956) 333–335.

[12] M.A.S. Azizi Samir, F. Alloin, M. Paillet, A. Dufresne, Tangling effect in fibrillated cellulose reinforced nanocomposites, Macromolecules. 37 (2004) 4313–4316.

[13] S. Elazzouzi-Hafraoui, Y. Nishiyama, J.-L. Putaux, L. Heux, F. Dubreuil, C. Rochas, The Shape and Size Distribution of Crystalline Nanoparticles Prepared by Acid Hydrolysis of Native Cellulose, Biomacromolecules. 9 (2008) 57–65.

[14] Y. Habibi, A.-L. Goffin, N. Schiltz, E. Duquesne, P. Dubois, A. Dufresne, Bionanocomposites based on poly(ε-caprolactone)-grafted cellulose nanocrystals by ring-opening polymerization, J. Mater. Chem. 18 (2008) 5002–5010.

[15] B.L. Peng, N. Dhar, H.L. Liu, K.C. Tam, Chemistry and applications of nanocrystalline cellulose and its derivatives: A nanotechnology perspective, The Canadian Journal of Chemical Engineering. 89 (2011) 1191–1206.

[16] P. Lu, Preparation and properties of cellulose nanocrystals: Rods, spheres, and network, Carbohydrate Polymers. 82 (2010) 329–336.

[17] J.F. Revol, H. Bradford, J. Giasson, R.H. Marchessault, D.G. Gray, Helicoidal self-ordering of cellulose microfibrils in aqueous suspension, International Journal of Biological Macromolecules. 14 (1992) 170–172.

[18] J. Araki, M. Wada, S. Kuga, Steric Stabilization of a Cellulose Microcrystal Suspension by Poly(ethylene glycol) Grafting, Langmuir. 17 (2001) 21–27.

[19] M.N. Anglès, A. Dufresne, Plasticized Starch/Tunicin Whiskers Nanocomposites. 1. Structural Analysis, Macromolecules. 33 (2000) 8344–8353.

[20] M.M. De Souza Lima, J.T. Wong, M. Paillet, R. Borsali, R. Pecora, Translational and Rotational Dynamics of Rodlike Cellulose Whiskers, Langmuir. 19 (2003) 24–29.

[21] M. Grunert, W.T. Winter, Nanocomposites of Cellulose Acetate Butyrate Reinforced with Cellulose Nanocrystals, Journal of Polymers and the Environment. 10 (2002) 27–30.

[22] N.L. Garcia de Rodriguez, W. Thielemans, A. Dufresne, Sisal cellulose whiskers reinforced polyvinyl acetate nanocomposites, Cellulose. 13 (2006) 261–270.

[23] K. Fleming, D. Gray, S. Prasannan, S. Matthews, Cellulose Crystallites: A New and Robust Liquid Crystalline Medium for the Measurement of Residual Dipolar Couplings, J. Am. Chem. Soc. 122 (2000) 5224–5225.

[24] S. Kalia, A. Dufresne, B.M. Cherian, B.S. Kaith, L. Avérous, J. Njuguna, et al., Cellulose-Based Bio- and Nanocomposites: A Review, International Journal of Polymer Science. 2011 (2011) 1–35.

[25] J. Araki, S. Kuga, Effect of Trace Electrolyte on Liquid Crystal Type of Cellulose Microcrystals, Langmuir. 17 (2001) 4493–4496.

[26] G. Siqueira, J. Bras, A. Dufresne, Luffa cylindrica as a lignocellulosic source of fiber, microfibrillated cellulose, and cellulose nanocrystals, BioResources. 5 (2010) 727–726.

[27] L. Pranger, R. Tannenbaum, Biobased Nanocomposites Prepared by In Situ Polymerization of Furfuryl Alcohol with Cellulose Whiskers or Montmorillonite Clay, Macromolecules. 41 (2008) 8682–8687.

[28] I. Kvien, B.S. Tanem, K. Oksman, Characterization of cellulose whiskers and their nanocomposites by atomic force and electron microscopy, Biomacromolecules. 6 (2005) 3160–3165.

[29] W. Helbert, J.Y. Cavaillé, A. Dufresne, Thermoplastic nanocomposites filled with wheat straw cellulose whiskers. Part I: Processing and mechanical behavior, Polymer Composites. 17 (1996) 604–611.

[30] D. Viet, S. Beck-Candanedo, D.G. Gray, Dispersion of cellulose nanocrystals in polar organic solvents, Cellulose. 14 (2007) 109–113.

[31] X.M. Dong, D.G. Gray, Effect of Counterions on Ordered Phase Formation in Suspensions of Charged Rodlike Cellulose Crystallites, Langmuir. 13 (1997) 2404–2409.

[32] S. Beck, J. Bouchard, R. Berry, Dispersibility in Water of Dried Nanocrystalline Cellulose, Biomacromolecules. 13 (2012) 1486–1494.

[33] Y. Habibi, H. Chanzy, M.R. Vignon, TEMPO-mediated surface oxidation of cellulose whiskers, Cellulose. 13 (2006) 679–687.

[34] M. Hasani, E.D. Cranston, G. Westman, D.G. Gray, Cationic surface functionalization of cellulose nanocrystals, Soft Matter. 4 (2008) 2238–2244.

[35] Goussé C., Chanzy H., Excoffier G., Soubeyrand L., Fleury E., Stable suspensions of partially silylated cellulose whiskers dispersed in organic solvents, Polymer. 43 (2002) 2645–2651.

[36] A. Junior de Menezes, G. Siqueira, A.A.S. Curvelo, A. Dufresne, Extrusion and characterization of functionalized cellulose whiskers reinforced polyethylene nanocomposites, Polymer. 50 (2009) 4552–4563.

[37] J. K. Pandey, W.S. Chu, C.S. Kim, C.S. Lee, S.H. Ahn, Bio-nano reinforcement of environmentally degradable polymer matrix by cellulose whiskers from grass, Composites Part B: Engineering. 40 (2009) 676–680.

[38] G. Siqueira, J. Bras, A. Dufresne, Cellulose Whiskers versus Microfibrils: Influence of the Nature of the Nanoparticle and its Surface Functionalization on the Thermal and Mechanical Properties of Nanocomposites, Biomacromolecules. 10 (2009) 425–432.

[39] E. Lam, K.B. Male, J.H. Chong, A.C.W. Leung, J.H.T. Luong, Applications of functionalized and nanoparticle-modified nanocrystalline cellulose, Trends in Biotechnology. 30 (2012) 283–290.

[40] J. O. Zoppe, Y. Habibi, O.J. Rojas, R.A. Venditti, L.-S. Johansson, K. Efimenko, et al., Poly(N-isopropylacrylamide) Brushes Grafted from Cellulose Nanocrystals via

Surface-Initiated Single-Electron Transfer Living Radical Polymerization, Biomacromolecules. 11 (2010) 2683–2691.

[41] B. Zhao, W.J. Brittain, Polymer brushes: surface-immobilized macromolecules, Progress in Polymer Science. 25 (2000) 677–710.

[42] J. Yi, Q. Xu, X. Zhang, H. Zhang, Chiral-nematic self-ordering of rodlike cellulose nanocrystals grafted with poly(styrene) in both thermotropic and lyotropic states, Polymer. 49 (2008) 4406–4412.

[43] A. Carlmark, E. Larsson, E. Malmström, Grafting of cellulose by ring-opening polymerisation – A review, European Polymer Journal. 48 (2012) 1646–1659.

[44] M. A. C. Stuart, W.T.S. Huck, J. Genzer, M. Müller, C. Ober, M. Stamm, et al., Emerging applications of stimuli-responsive polymer materials, Nat Mater. 9 (2010) 101–113.

[45] P. Bawa, V. Pillay, Y.E. Choonara, L.C. du Toit, Stimuli-responsive polymers and their applications in drug delivery, Biomed Mater. 4 (2009) 022001.

[46] K.C. Gupta, K. Khandekar, Temperature-Responsive Cellulose by Ceric(IV) Ion-Initiated Graft Copolymerization of N-Isopropylacrylamide, Biomacromolecules. 4 (2003) 758–765.

[47] L.Q. Wang, K. Tu, Y. Li, J. Zhang, L. Jiang, Z. Zhang, Synthesis and characterization of temperature responsive graft copolymers of dextran with poly(N-isopropylacrylamide), Reactive and Functional Polymers. 53 (2002) 19–27.

[48] Y.N. Liu, H.Y. Yu, Z.Y. Qin, L. Chen, Enhanced Heat Conduction in Cellulose Nanocrystals Grafting Polyethylene Glycol as Solid-Solid Phase Change Materials, Advanced Materials Research. 557-559 (2012) 563–566.

[49] A.E. Way, L. Hsu, K. Shanmuganathan, C. Weder, S.J. Rowan, pH-Responsive Cellulose Nanocrystal Gels and Nanocomposites, ACS Macro Lett. 1 (2012) 1001–1006.

[50] N. Işıklan, M. İnal, F. Kurşun, G. Ercan, pH responsive itaconic acid grafted alginate microspheres for the controlled release of nifedipine, Carbohydrate Polymers. 84 (2011) 933–943.

[51] Y. Xie, C. Yuan, Visible-light responsive cerium ion modified titania sol and nanocrystallites for X-3B dye photodegradation, Applied Catalysis B: Environmental. 46 (2003) 251–259.

[52] J.T. Koberstein, Molecular design of functional polymer surfaces, Journal of Polymer Science Part B: Polymer Physics. 42 (2004) 2942–2956.

[53] J. Draper, I. Luzinov, S. Minko, I. Tokarev, M. Stamm, Mixed Polymer Brushes by Sequential Polymer Addition: Anchoring Layer Effect, Langmuir. 20 (2004) 4064–4075.

[54] M. Motornov, Stimuli-Responsive Colloidal Systems from Mixed Brush-Coated Nanoparticles, Advanced Functional Materials. 17 (2007) 2307–2314.

[55] O. Azzaroni, UCST Wetting Transitions of Polyzwitterionic Brushes Driven by Self-Association, Angewandte Chemie International Edition. 45 (2006) 1770–1774.

[56] T. Wu, P. Gong, I. Szleifer, P. Vlček, V. Šubr, J. Genzer, Behavior of Surface-Anchored Poly(acrylic acid) Brushes with Grafting Density Gradients on Solid Substrates: 1. Experiment, Macromolecules. 40 (2007) 8756–8764.

[57] C. Xu, T. Wu, C.M. Drain, J.D. Batteas, M.J. Fasolka, K.L. Beers, Effect of Block Length on Solvent Response of Block Copolymer Brushes: Combinatorial Study with Block Copolymer Brush Gradients, Macromolecules. 39 (2006) 3359–3364.

[58] H.G. Schild, Poly(N-isopropylacrylamide): experiment, theory and application, Progress in Polymer Science. 17 (1992) 163–249.

[59] S.Y. Lin, Thermal micro ATR/FT-IR spectroscopic system for quantitative study of the molecular structure of poly(N-isopropylacrylamide) in water, Polymer. 40 (1999) 2619–2624.

[60] K.C. Tam, Viscometry-a useful tool for studying conformational changes of poly(N-isopropylacrylamide) in solutions, Polymer. 33 (n.d.) 436–438.

[61] R. Pelton, Poly(N-isopropylacrylamide) (PNIPAM) is never hydrophobic, J Colloid Interface Sci. 348 (2010) 673–674.

[62] F.J. Xu, S.P. Zhong, L.Y.L. Yung, E.T. Kang, K.G. Neoh, Surface-Active and Stimuli-Responsive Polymer−Si(100) Hybrids from Surface-Initiated Atom Transfer Radical Polymerization for Control of Cell Adhesion, Biomacromolecules. 5 (2004) 2392–2403.

[63] I. Lokuge, X. Wang, P.W. Bohn, Temperature-Controlled Flow Switching in Nanocapillary Array Membranes Mediated by Poly(N-isopropylacrylamide) Polymer Brushes Grafted by Atom Transfer Radical Polymerization, Langmuir. 23 (2007) 305–311.

[64] H. Iwata, I. Hirata, Y. Ikada, Atomic Force Microscopic Images of Solvated Polymer Brushes, Langmuir. 13 (1997) 3063–3066.

[65] J. Lindqvist, D. Nyström, E. Östmark, P. Antoni, A. Carlmark, M. Johansson, et al., Intelligent Dual-Responsive Cellulose Surfaces via Surface-Initiated ATRP, Biomacromolecules. 9 (2008) 2139–2145.

[66] W. Zhang, L. Shi, R. Ma, Y. An, Y. Xu, K. Wu, Micellization of Thermo- and pH-Responsive Triblock Copolymer of Poly(ethylene glycol)-b-poly(4-vinylpyridine)-b-poly(N-isopropylacrylamide), Macromolecules. 38 (2005) 8850–8852.

[67] F. Azzam, L. Heux, J.-L. Putaux, B. Jean, Preparation By Grafting Onto, Characterization, and Properties of Thermally Responsive Polymer-Decorated Cellulose Nanocrystals, Biomacromolecules. 11 (2010) 3652–3659.

[68] W. Agut, A. Brûlet, D. Taton, S. Lecommandoux, Thermoresponsive Micelles from Jeffamine-b-poly(l-glutamic acid) Double Hydrophilic Block Copolymers, Langmuir. 23 (2007) 11526–11533.

[69] J.O. Zoppe, M. Osterberg, R.A. Venditti, J. Laine, O.J. Rojas, Surface interaction forces of cellulose nanocrystals grafted with thermoresponsive polymer brushes, Biomacromolecules. 12 (2011) 2788–2796.

[70] J.O. Zoppe, R.A. Venditti, O.J. Rojas, Pickering emulsions stabilized by cellulose nanocrystals grafted with thermo-responsive polymer brushes, J Colloid Interface Sci. 369 (2012) 202–209.

[71] E. Kloser, D.G. Gray, Surface Grafting of Cellulose Nanocrystals with Poly(ethylene oxide) in Aqueous Media, Langmuir. 26 (2010) 13450–13456.

[72] A.P. Mangalam, J. Simonsen, A.S. Benight, Cellulose/DNA Hybrid Nanomaterials, Biomacromolecules. 10 (2009) 497–504.

[73] A.Y. Denisov, E. Kloser, D.G. Gray, A.K. Mittermaier, Protein alignment using cellulose nanocrystals: practical considerations and range of application, J Biomol NMR. 47 (2010) 195–204.

[74] A. Dorris, D.G. Gray, Gelation of cellulose nanocrystal suspensions in glycerol, Cellulose. 19 (2012) 687–694.

[75] R. Cha, Z. He, Y. Ni, Preparation and characterization of thermal/pH-sensitive hydrogel from carboxylated nanocrystalline cellulose, Carbohydrate Polymers. 88 (2012) 713–718.

[76] A. Šturcová, G.R. Davies, S.J. Eichhorn, Elastic Modulus and Stress-Transfer Properties of Tunicate Cellulose Whiskers, Biomacromolecules. 6 (2005) 1055–1061.

[77] V. Favier, G.R. Canova, J.Y. Cavaillé, H. Chanzy, A. Dufresne, C. Gauthier, Nanocomposite materials from latex and cellulose whiskers, Polymers for Advanced Technologies. 6 (1995) 351–355.

[78] N. Lin, J. Huang, P.R. Chang, J. Feng, J. Yu, Surface acetylation of cellulose nanocrystal and its reinforcing function in poly(lactic acid), Carbohydrate Polymers. 83 (2011) 1834–1842.

[79] J.R. Capadona, K. Shanmuganathan, D.J. Tyler, S.J. Rowan, C. Weder, Stimuli-Responsive Polymer Nanocomposites Inspired by the Sea Cucumber Dermis, Science. 319 (2008) 1370–1374.

[80] L. Hsu, C. Weder, S.J. Rowan, Stimuli-responsive, mechanically-adaptive polymer nanocomposites, J. Mater. Chem. 21 (2011) 2812–2822.

[81] K. Shanmuganathan, J.R. Capadona, S.J. Rowan, C. Weder, Stimuli-Responsive Mechanically Adaptive Polymer Nanocomposites, ACS Appl. Mater. Interfaces. 2 (2010) 165–174.

[82] J. Fox, J.J. Wie, B.W. Greenland, S. Burattini, W. Hayes, H.M. Colquhoun, et al., High-Strength, Healable, Supramolecular Polymer Nanocomposites, J. Am. Chem. Soc. 134 (2012) 5362–5368.

[83] M.V. Biyani, E.J. Foster, C. Weder, Light-Healable Supramolecular Nanocomposites Based on Modified Cellulose Nanocrystals, ACS Macro Lett. 2 (2013) 236–240.

[84] D.J. McDowall, B.S. Gupta, V.T. Stannett, Grafting of vinyl monomers to cellulose by ceric ion initiation, Progress in Polymer Science. 10 (1984) 1–50.

[85] O.Y. Mansour, A. Nagaty, Grafting of synthetic polymers to natural polymers by chemical processes, Progress in Polymer Science. 11 (1985) 91–165.

[86] G. Mino, S. Kaizerman, A new method for the preparation of graft copolymers. Polymerization initiated by ceric ion redox systems, Journal of Polymer Science. 31 (1958) 242–243.

[87] E. Schwab, V. Stannett, Rakowitz, D. H, Magrane, J. K, Paper Grafted with Vinyl Monomers Using the Ceric Ion Method, TAPPI. 45 (1962) 390–400.

[88] A. Pourjavadi, M.J. Zohuriaan-Mehr, Modification of Carbohydrate Polymers via Grafting in Air. 2. Ceric-Initiated Graft Copolymerization of Acrylonitrile onto Natural and Modified Polysaccharides, Starch - Stärke. 54 (2002) 482–488.

[89] Y. Ogiwara, Y. Ogiwara, H. Kubota, Effects of carbonyl and aldehyde groups in the graft copolymerization of methyl methacrylate on cellulose with a ceric salt, Journal of Polymer Science A Polymer Chemistry. 5 (1967) 2791–2805.

[90] A.A. Katai, V.K. Kulshrestha, R.H. Marchessault, Ceric ion-initiated polymerization of acrylonitrile in the presence of alcohols, Journal of Polymer Science Part C: Polymer Symposia. 2 (1963) 403–414.

[91] M.M. Huque, M. Habibuddowla, A.J. Mahmood, A.J. Mian, Graft copolymerization onto jute fiber: Ceric ion-initiated graft copolymerization of methyl methacrylate, Journal of Polymer Science: Polymer Chemistry Edition. 18 (1980) 1447–1458.

[92] O.Y. Mansour, A. Nagaty, Some aspects of graft polymerization of vinyl monomers onto cellulose by use of tetravalent cerium. VI, Journal of Applied Polymer Science. 23 (1979) 2425–2434.

[93] Y. Iwakura, T. Kurosaki, K. Uno, Y. Imai, Reactive fiber. II. Chemical reactivities of cellulose fiber grafted with glycidyl methacrylate, Journal of Polymer Science Part C: Polymer Symposia. 4 (1963) 673–698.

[94] H.L. Hintz, D.C. Johnson, Mechanism of oxidation of cyclic alcohols by cerium (IV), J. Org. Chem. 32 (1967) 556–564.

[95] G. Mino, S. Kaizerman, E. Rasmussen, The oxidation of polyvinyl alcohol by ceric ion, Journal of Polymer Science. 39 (1959) 523–529.

[96] A.Y. Kulkarni, P.C. Mehta, Ceric ion-induced redox polymerization of acrylonitrile on cellulose, Journal of Applied Polymer Science. 12 (1968) 1321–1342.

[97] A. Hebeish, P.C. Mehta, Cerium-initiated grafting of acrylonitrile onto cellulosic materials, Journal of Applied Polymer Science. 12 (1968) 1625–1647.

[98] C.R. Pottenger, D.C. Johnson, Mechanism of cerium (IV) oxidation of glucose and cellulose, Journal of Polymer Science Part A-1: Polymer Chemistry. 8 (1970) 301–318.

[99] J.C. Arthur, P.J. Baugh, O. Hinojosa, ESR study of reactions of cellulose initiated by the ceric ion method, Journal of Applied Polymer Science. 10 (1966) 1591–1606.

[100] T. Taga, H. Inagaki, Graft Copolymerization of Vinyl Monomers onto Cellulose with eerie Ion: The Reducing Endgroup of Cellulose as the Grafting Site, Sen-i Gakkaishi (Journal of the Society of Fiber Science and Technology). 35 (1979) T512–T519.

[101] A.Y. Kulkarni, P.C. Mehta, Oxidation of cellulose by ceric ion, Journal of Polymer Science Part B: Polymer Letters. 5 (1967) 209–215.

[102] N. Gaylord, A proposed new mechanism for catalyzed and uncatalyzed graft polymerization onto cellulose, Journal of Polymer Science Part C: Polymer Symposia. 37 (1972) 153–172.

[103] N.G. Gaylord, Cellulose-monomer interaction and a revised mechanism for graft copolymerization, Journal of Macromolecular Science: Chemistry. v. A10(4) p. 737-757 (1976).

[104] H. Kamogawa, T. Sekiya, Graft Polymerization of Acrylamide onto Cotton Fabric for Further Treatments, Textile Research Journal. 31 (1961) 585–591.

[105] G.N. Richards, E.P.T. White, Graft polymerization on cellulosic materials. Part I. Cation-exchange membranes from paper and acrylic acid, Journal of Polymer Science Part C: Polymer Symposia. 4 (1963) 1251–1260.

[106] O.Y. Mansour, J. Schurz, Some aspects of graft polymerization of vinyl monomers onto cellulose using tetravalent cerium III, Svensk Papperstidn. 76 (1973) 415–418.

[107] O.Y. Mansour, A. Nagaty, Some aspects of graft polymerization of vinyl monomers onto cellulose by use of tetravalent cerium. IV, Journal of Polymer Science: Polymer Chemistry Edition. 12 (1974) 141–152.

[108] P. Lepoutre, S.H. Hui, Grafting acrylonitrile onto wood pulp: Influence of process variables, Journal of Applied Polymer Science. 19 (1975) 1257–1268.

[109] A. Bazuaye, F.E. Okieimen, O.B. Said, Some aspects of graft copolymerization of acrylonitrile onto holocellulose, Acta Polymerica. 40 (1989) 126–128.

[110] E.F. Okieimen, J.E. Ebhoaye, Grafting acrylonitrile and acrylic acid monomers on cellulosic materials, Journal of Applied Polymer Science. 31 (1986) 1275–1280.

[111] K.C. Gupta, S. Sahoo, Graft Copolymerization of Acrylonitrile and Ethyl Methacrylate Comonomers on Cellulose Using Ceric Ions, Biomacromolecules. 2 (2001) 239–247.

[112] K.C. Gupta, S. Sahoo, K. Khandekar, Graft Copolymerization on to Cellulose Using Binary Mixture of Monomers, Journal of Macromolecular Science, Part A. 44 (2007) 707–719.

[113] H. Narita, S. Machida, Graft Copolymerization of Acrylamide Onto Microcrystalline Cellulose, Sen-i Gakkaishi (Journal of the Society of Fiber Science and Technology). 27 (1971) 162–167.

[114] E.D. Cranston, D.G. Gray, Morphological and Optical Characterization of Polyelectrolyte Multilayers Incorporating Nanocrystalline Cellulose, Biomacromolecules. 7 (2006) 2522–2530.

[115] L. Bergström, S. Stemme, T. Dahlfors, H. Arwin, L. Ödberg, Spectroscopic Ellipsometry Characterisation and Estimation of the Hamaker Constant of Cellulose, Cellulose. 6 (1999) 1–13.

[116] L. Ma, H. Kang, R. Liu, Y. Huang, Smart assembly behaviors of hydroxypropylcellulose-graft-poly(4-vinyl pyridine) copolymers in aqueous solution by thermo and pH stimuli, Langmuir. 26 (2010) 18519–18525.

[117] G.S. Chauhan, B. Singh, S.K. Dhiman, Functionalization of poly(4-vinyl pyridine) grafted cellulose by quaternization reactions and a study on the properties of postquaternized copolymers, Journal of Applied Polymer Science. 91 (2004) 2454–2464.

[118] S.N. Bhattacharyya, D. Maldas, Graft copolymerization onto cellulosics, Progress in Polymer Science. 10 (1984) 171–270.

[119] Y. Onishi, 1,2-propanediol–cellulose–acrylamide graft copolymers, Journal of Applied Polymer Science. 92 (2004) 3022–3029.

[120] F.E. Okieimen, D.E. Ogbeifun, Graft copolymerizations of modified cellulose: Grafting of methyl acrylate, ethyl acrylate and ethyl methacrylate on carboxy methyl cellulose, European Polymer Journal. 32 (1996) 311–315.

[121] T.A. Dankovich, Contact Angle Measurements on Smooth Nanocrystalline Cellulose (I) Thin Films, Journal of Adhesion Science and Technology. 25 (2011) 699–708.

[122] I. Dierking, Textures of Liquid Crystals, John Wiley & Sons, 2003.

[123] J. Yi, Temperature-induced chiral nematic phase changes of suspensions of poly(*N*,*N*-dimethylaminoethyl methacrylate)-grafted cellulose nanocrystals, Cellulose. 16 (2009) 989–997.

[124] Y. Nishiyama, P. Langan, H. Chanzy, Crystal Structure and Hydrogen-Bonding System in Cellulose Iβ from Synchrotron X-ray and Neutron Fiber Diffraction, J. Am. Chem. Soc. 124 (2002) 9074–9082.

[125] Y. Cui, C. Tao, Y. Tian, Q. He, J. Li, Synthesis of PNIPAM-co-MBAA copolymer nanotubes with composite control, Langmuir. 22 (2006) 8205–8208.

[126] M. Heskins, J.E. Guillet, Solution Properties of Poly(N-isopropylacrylamide), Journal of Macromolecular Science: Part A - Chemistry. 2 (1968) 1441–1455.

[127] S. Fujishige, K. Kubota, I. Ando, Phase transition of aqueous solutions of poly(N-isopropylacrylamide) and poly(*N*-isopropylmethacrylamide), J. Phys. Chem. 93 (1989) 3311–3313.

[128] A. Matsuyama, F. Tanaka, Theory of solvation-induced reentrant phase separation in polymer solutions, Phys. Rev. Lett. 65 (1990) 341–344.

[129] M.R. Mauricio, Analysis of poly(*N*-isopropylacrylamide) grafted onto the surface of PET films by SI-ATRP technique, Materials Science & Engineering C. 29 (2009) 594–598.

[130] W. Wang, “Smart” membrane materials: Preparation and characterization of PVDF-g-PNIPAAm graft copolymer, Journal of Applied Polymer Science. 104 (2007) 1482–1486.

[131] P.W. Atkins, J. de Paula, Atkins’ Physical Chemistry, 8th ed., W.H. Freeman & Company, 2006.